



HAL
open science

Printing quality control of cement-based materials under flow and rest conditions

Ilhame Harbouz, Ammar Yahia, Emmanuel Rozière, Ahmed Loukili

► To cite this version:

Ilhame Harbouz, Ammar Yahia, Emmanuel Rozière, Ahmed Loukili. Printing quality control of cement-based materials under flow and rest conditions. *Cement and Concrete Composites*, 2023, 138, pp.104965. 10.1016/j.cemconcomp.2023.104965 . hal-04406488

HAL Id: hal-04406488

<https://hal.science/hal-04406488>

Submitted on 13 Mar 2024

HAL is a multi-disciplinary open access archive for the deposit and dissemination of scientific research documents, whether they are published or not. The documents may come from teaching and research institutions in France or abroad, or from public or private research centers.

L'archive ouverte pluridisciplinaire **HAL**, est destinée au dépôt et à la diffusion de documents scientifiques de niveau recherche, publiés ou non, émanant des établissements d'enseignement et de recherche français ou étrangers, des laboratoires publics ou privés.

1 Printing Quality Control of Cement-based Materials under Flow 2 and Rest Conditions

3 Ilhame HARBOUZ ^{1,2}, Ammar YAHIA ¹, Emmanuel ROZIERE ², Ahmed LOUKILI ²

4 ¹ Université de Sherbrooke, Department of Building and Civil Engineering, Sherbrooke, J1K 2R1, Québec, Canada

5 ² Nantes Université, Ecole Centrale Nantes, CNRS, GeM, UMR 6183, 44000 Nantes, France

6 Abstract

7 Time-dependent rheological properties of cement-based materials have a significant impact on
8 3D printing processes, where multiple rheological requirements should be met. A proper high
9 rate of structural build-up is recommended to ensure the buildability and stability of printed
10 elements. However, the loss of workability may occur rapidly, resulting in a significant reduction
11 in print quality. Workability and buildability requirements usually interfere due to the time-
12 dependent rheological behavior of cement-based materials under flow and rest conditions. This
13 research aims to highlight the effects of time-dependent behavior on the printability of cement-
14 based materials. The coupling mechanisms of microstructure development at rest and under
15 shearing conditions are discussed. A new thixotropy index is proposed to quantify the
16 printability window of cement-based materials based on their structuration rates. An
17 experimental study was conducted on printable mortars incorporating a viscosity-modifying
18 agent (VMA) to assess printing quality as a function of the degree of thixotropy. Different types
19 of stability failures were captured and discussed.

20 **Keywords:** 3D printing, buildability, breakdown, build-up, cement-based materials, flow,
21 flocculation, rigidification, structuration, time-dependent behavior, thixotropy

22 Notations

23 Material properties

- 24 • μ_p is the plastic viscosity [Pa.s];
- 25 • $\tau_d(t)$ or τ_d is the minimum shear stress to maintain flow [Pa], while $\tau_{d,0}$ is the initial
26 dynamic yield stress [Pa];
- 27 • c is the pseudoplastic index based on the Modified Bingham model [Pa.s²];
- 28 • β is the dynamic structuration [Pa/min];
- 29 • $A_{\text{breakdown}}$ and A_{buildup} are the break-down and build-up areas, respectively [Pa/s];
- 30 • t_{fl} is the workability period [min];
- 31 • $\dot{\gamma}_c$ is the minimum shear rate to maintain the break-down of the structure [1/s];

- 32 • t_{trans} is the transitional period between the break-down structure-dominated phase and
- 33 the build-up structure-dominated one [min];
- 34 • $\tau_{d,\text{eq}}$ is the equilibrium value of dynamic yield stress determined using the flow onset
- 35 curve [Pa] and β_{eq} is its evolution rate [Pa/min];
- 36 • $\tau_s(t)$ or τ_s is the static yield stress of the printed material while $\tau_{s,\text{floc}}$ is the initial static
- 37 yield stress after the re-flocculation period [Pa];
- 38 • G is the elastic shear modulus [Pa];
- 39 • t_{rf} is the re-flocculation period [min];
- 40 • t'_c is the period over which non-linear structuration occurs **at rest** [min];
- 41 • t_c is the transitional period between linear and non-linear structurations, referred to as
- 42 open time [min] ($t_c = \min(t_{\text{fl}}, t'_c)$);
- 43 • $G'(t)$ is the storage modulus, G'_0 is the initial storage modulus and G'_{floc} is its value after
- 44 the re-flocculation period [Pa];
- 45 • R_{thix} and A_{thix} are the re-flocculation and the structuration rates, respectively [Pa/min];
- 46 • ρ is the density [kg/m^3];
- 47 • $\gamma_{\text{lim}} = G(t)/\rho gh$ is the maximum deformation that the printable material can tolerate
- 48 before failure.

49 Printing parameters

- 50 • $P_{\text{pump/extrusion}}$ is the pumping/extrusion pressure [bar];
- 51 • h_t is the height of the deposited layer at printing time t [m];
- 52 • $h(t) = R \cdot t$ is the printed object height during printing time ' t ' [m], while R is the vertical
- 53 rising of the printed object height [m/s].
- 54 • w_{design} is the width of the print layer [m];

55 Printing failure parameters

- 56 • w_c is the critical width causing the stability-failure of the printed structure [m];
- 57 • h_c is the critical object height, at which self-buckling of the printed object is expected
- 58 [m].

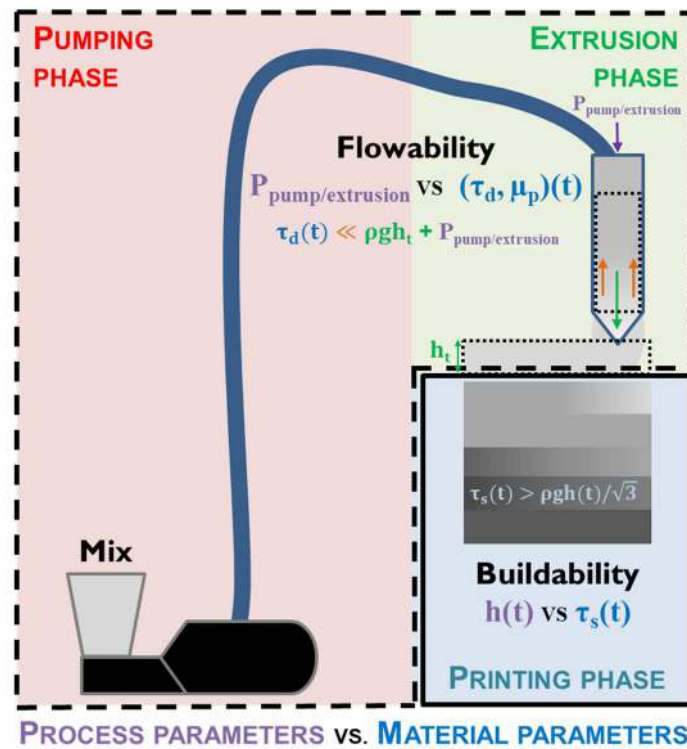
59 **1. Introduction**

60 Concrete 3D printing is an emerging technology that will have a considerable impact on the
 61 construction industry in the near future. 3D printing has tremendous potential for offering great
 62 architectural design freedom, speeding up the construction process, and reducing the
 63 construction time, cost, and waste while achieving a greater degree of customization [1–5]. The
 64 absence of conventional formworks and the layer-wise pressure increase in concrete 3D printing
 65 require designing materials with an adapted structuration rate. This is commonly referred to as
 66 the buildability of cement-based materials used for 3D printing applications [6,7]. However, the
 67 rheological requirements imposed by the printing process are challenging and necessitate careful
 68 design and material selection to achieve adequate properties for 3D printed structures [8]. In
 69 addition to good buildability, the print material requires adequate flowability to facilitate both

70 pumping and extrusion processes. Buildability refers to the ability of the print materials to carry
71 subsequent layers without collapsing, as shown in **Fig.1**. Therefore, flowability and buildability
72 are essential for a successful printability of the material.

73 Fresh cementitious materials are thixotropic and exhibit time-dependent behavior with yield
74 stress. These properties play a significant role in pumping, formwork pressure, and multilayer
75 casting. Under shearing, these materials may undergo a shear thinning or a shear thickening
76 behavior depending on the applied shear regime [9]. It is worthy to mention that in 3D printing
77 applications, shear-thickening behavior is undesirable due to potential blockage problems that
78 may arise during extrusion. The time-dependent character alters the printability of cement-based
79 suspensions [4]. This mainly depends on the mixture composition, mixing energy, mode of
80 production, and the printing process. The solid fraction (i.e. water-to-cement ratio), the type and
81 content of binder, type and dosage of admixtures, and temperature are among the most important
82 mixture parameters. The mode of production includes continuous production, multi-batch, or
83 single-batch productions. Continuous production is usually used in large-scale processes, while
84 multi-batches or single batch modes are used for small-scale applications in the laboratory. The
85 mode of production can affect the time-dependent aspect, which can lead to cold joint
86 appearance, cracks, and flow instability. Furthermore, the extrusion device (e.g. gravitation,
87 screw-extrusion, etc.) and the mode of deposition (e.g. free-flow deposition, infinite-brick, etc.)
88 may necessitate different rheological requirements to ensure good printability of the material [3]
89 (**Table 1**). In this regard, the distinction between flowable and stiffer materials has been
90 proposed in the literature [10,11]. Flowable materials are those commonly used in free-flow
91 deposition processes, while stiffer ones are used in infinite-brick extrusion [12]. This
92 classification is mainly based on an empirical evaluation and does not allow a fundamental
93 understanding of the interfering mechanisms behind the time-dependent rheological behavior of
94 printable materials **at rest** (during the deposition phase) and **under shear conditions** (during
95 pumping and extrusion phases). Besides, the transition from a flowable state to a stiffer one can
96 be extremely fast during printing. Proposing a rheological index to properly describe the time-
97 dependent behavior of print materials is necessary to allow a better understanding of the
98 rheological behavior of print materials at different stages of the printing process. In this study, a
99 new thixotropy index is defined for better evaluation of the material's printability window. The
100 proposed index has been adapted to different printing modes. A case study was conducted on
101 four printable mixtures of different rheological properties to evaluate the consequences of the
102 time-dependent rheological behavior on the printing quality. Furthermore, the effect of a

103 viscosity-modifying admixture (VMA) on the structuration of printable cement-based materials
 104 was also evaluated. The flow and the structural build-up properties of the investigated mixtures
 105 have been determined. The structuration rates were used to predict the failure of the printed
 106 elements based on strength stability conditions, following the von Mises plasticity criterion [1,8],
 107 as shown in **Fig. 1**. Finally, printing tests were performed at different ages to assess the variation
 108 of the printing quality over time and assess the adequacy of the printing criteria.



109

110 **Fig. 1:** The main steps of extrusion-based 3D printing and the relevant associated parameters

111 **Table 1:** The ranges of rheological properties of cement-based materials used in extrusion-based
 112 printing processes

Extrusion process	Extrusion with setting activation	Infinite-brick extrusion	Free flow deposition (without stirring)	Free flow deposition (with stirring)
$\tau_{d,0}$	$10 \text{ Pa} \leq \tau_{d,0} \leq 100 \text{ Pa}$	$\tau_{d,0} > 100 \text{ Pa}$ [3]	$10 \text{ Pa} \leq \tau_{d,0} \leq 500 \text{ Pa}$ [3,13]	
$\tau_{s,0}$	$\tau_{s,0} > 1 \text{ kPa}$ [14,15]	$\tau_{s,0} > 500 \text{ Pa}$ [3]	$\tau_{s,0} > 500 \text{ Pa}$ [16,17]	$\tau_{s,0} \geq 150 \text{ Pa}$ [18,19]
A_{thix}	$A_{\text{thix}} > 100 \text{ Pa/min}$ [14,15]	$A_{\text{thix}} > 20 \text{ Pa/min}$ [3]	$A_{\text{thix}} > 20 \text{ Pa/min}$ [16,20]	$A_{\text{thix}} \leq 20 \text{ Pa/min}$ [19]
Classification	N/A	Stiff [3]	Flowable [3]	

113 2. Theoretical framework

114 Printable materials must ensure good workability during the pumping and extrusion phases, as
 115 well as adequate stability during the deposition process. Between the two phases, the material
 116 undergoes a transition from liquid-like (during pumping) to solid-like (after deposition).
 117 Understanding such transition can help in overcoming challenges during the printing process and
 118 ensuring good printing quality.

119 2.1. Flow behavior

120 Cement-based materials generally do not flow unless they are subjected to critical stress to
 121 overcome the internal structure. If the material displays a shear-thinning behavior, this value
 122 decreases as the material breaks down until reaching an equilibrium shear stress (τ_d) (also known
 123 as dynamic yield stress). This threshold shear stress must be maintained to ensure the pumping
 124 and extrusion of the material, which mainly depends on the printing scale and its technical
 125 features (**Table 1**). Under a given shearing regime, two kinetic processes occur simultaneously,
 126 including the break-down caused by hydrodynamic forces and build-up due to flocculation
 127 mechanisms [21]. Shearing does not only break down flocs but also induces flocculation, which
 128 is referred to as orthokinetic flocculation [22,23]. The steady-state flow behavior corresponds to
 129 a balance between the two processes. The resulting equilibrium structure will depend on both the
 130 age of the mixture and the applied shear rate, which tends towards greater breakdown at higher
 131 shear rates. In this paper, the competition between the two processes will be evaluated by
 132 considering the hysteresis loop, which will be detailed in **section 3**.

133 Moreover, due to the hydration, an irreversible structuration occurs with time, which can be
 134 expressed by an exponential increase [24,25]. This leads to flow loss, hence impeding the
 135 pumping and extrusion of the material [8]. Because of their relatively high structuration rate, the
 136 printable cement-based materials can exhibit a quick flow loss in a shorter time. In this case, the
 137 evolution of the dynamic yield stress must be considered to control the printing quality during
 138 the pumping and extrusion phases. Wang et al. [26] have proposed an exponential model to
 139 describe the time evolution of the dynamic yield stress based on structural kinetic constitutive
 140 models detailed in [24] (**Eq. (1)**), as follows:

$$141 \quad \tau_d(t) = \tau_{d,0} + \beta_{thix} \cdot t_{fl}(e^{t/t_{fl}} - 1) \quad (1)$$

142 where $\tau_{d,0}$ represents the initial dynamic yield stress, t_{fl} indicates the beginning of the flow loss
 143 which is adjusted to obtain the best fit with experimental values, and β_{thix} is the dynamic

144 structuration of yield stress. By considering only the linear structuration, the equation **Eq. (1)** can
 145 be expressed as follows:

$$146 \quad \tau_d(t) = \tau_{d,0} + \beta_{thix} \cdot t \quad (2)$$

147 In order to maintain the extrudability of the print material, the dynamic yield stress should be
 148 overcome by the extrusion force and gravity throughout the printing time, as shown in **Eq. (3)**.
 149 Thus, the extrusion/pumping pressure should be adjusted considering the dynamic structuration
 150 of cement-based materials.

$$151 \quad \tau_d(t) < \rho g h_t + P_{pump/extrusion} \quad (3)$$

152 **2.2. Buildability**

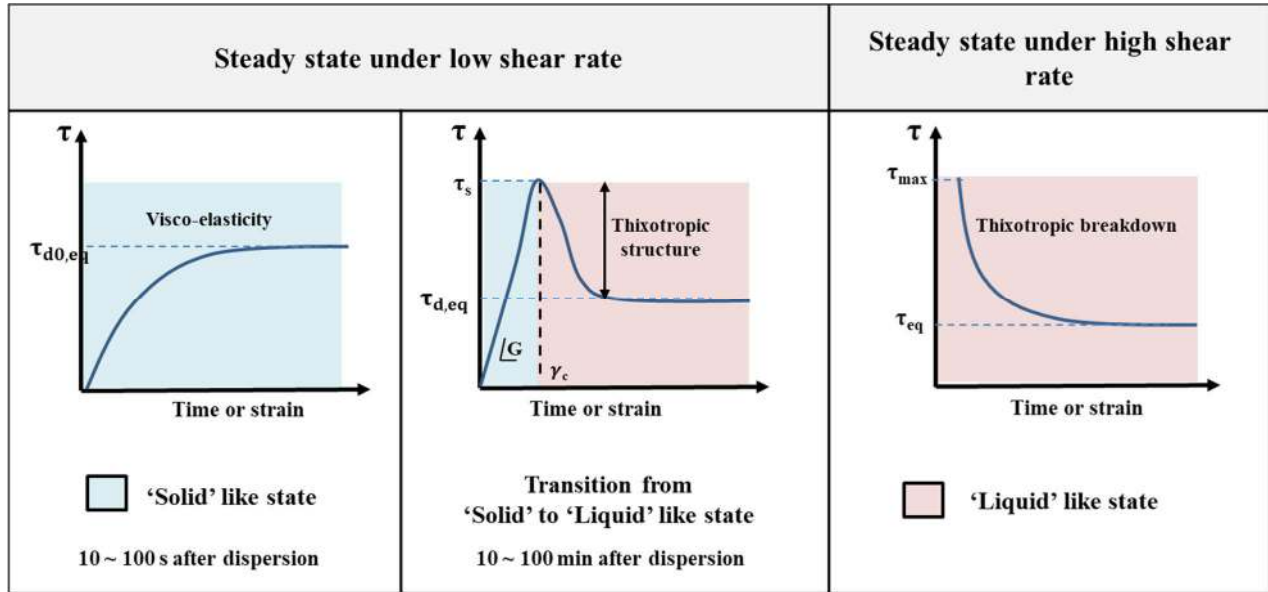
153 The buildability of cement-based material is an important property in assessing its suitability for
 154 printing. It is important to mention that this property depends on the material's characteristics,
 155 the geometry of the printed element (i.e., pattern), and the printing parameters (e.g. printing and
 156 extrusion speeds) [3]. From a material point of view, buildability is generally related to the
 157 structuration kinetics of the material at rest. Several approaches have been reported to evaluate
 158 the evolution of structural build-up of cement-based materials [11,27–30]. Most often, the
 159 evolution of static yield stress or storage modulus over time is employed. The most commonly
 160 used models to evaluate the structural build-up of printable cement-based materials are discussed
 161 in the following sections.

162 ***a) Flow onset behavior***

163 The most commonly used method to assess the static yield stress development of printable
 164 materials consists in evaluating their flow onset behavior using the constant shear rate (CSR) test
 165 [31–33]. This test involves applying a low shear rate after breaking down the internal network
 166 structure. During the stress relaxation, the microstructure should recover to its new steady state
 167 level after a characteristic time. In the case of cement-based materials, there exists a competition
 168 between the viscoelasticity and the thixotropic effects. The material response may then differ
 169 depending on the age of the mixture, the test duration, and the magnitude of the applied shear
 170 rate [34]. Immediately after mixing, if the applied shear rate is low enough to avoid any
 171 breakdown of the structure, the most expected response would be a gradual increase in stress,
 172 reflecting the viscoelasticity of the material, until reaching an equilibrium steady state (**Table 2**).
 173 At rest, a structure can be formed due to thixotropy, and an overshoot stress response is
 174 observed, reflected by a peak representing the static yield stress (τ_s), and followed by

175 breakdown until reaching an equilibrium shear stress ($\tau_{d,eq}$) [35], as shown in **Table 2**. The
 176 strain corresponding to the maximum stress is the critical strain that marks the transition from a
 177 solid to a liquid-like state. The slope of the linear increase of the stress growth curve represents
 178 the elastic shear modulus G .

179 **Table 2:** Different transient steady flow behavior depending on the applied shear rate and resting
 180 time



181
 182 Kruger et al. [35] attributed the initial thixotropic response to the reversible particle flocculation
 183 process, characterized by the rapid re-flocculation rate (R_{thix}), which occurs within the first few
 184 hundred seconds after removing external energy. The R_{thix} coefficient can be calculated using
 185 **Eq. (4)**, as follows:

$$186 \quad R_{thix} = \frac{\tau_{s,0} - \tau_{d,eq0}}{t_{rf}} \quad (4)$$

187 where $\tau_{s,0}$ is the initial static yield stress (Pa), $\tau_{d,eq0}$ is the initial equilibrium stress measured in
 188 the CSR test (Pa), and t_{rf} is the period over which re-flocculation occurs and dominates shear
 189 stress increase. The rapid re-flocculation process is mainly governed by the orthokinetic,
 190 perikinetic aggregation, and differential sedimentation resulting from shear-induced forces,
 191 Brownian motion, and particle collisions, respectively, due to differences in the settling
 192 velocities [21,35]. The resulted structure evolves linearly [36] and tends to deviate from linearity
 193 to an exponential trend due to irreversible structuration [11]. As a result, the time evolution of
 194 the static yield stress can be expressed according to **Eq. (5)**:

$$195 \quad \tau_s(t) = \tau_{s,floc} + A_{thix} \cdot t_c (e^{t/t_c} - 1) \xrightarrow{\text{linear domain}} \tau_{s,floc} + A_{thix} \cdot t \quad (5)$$

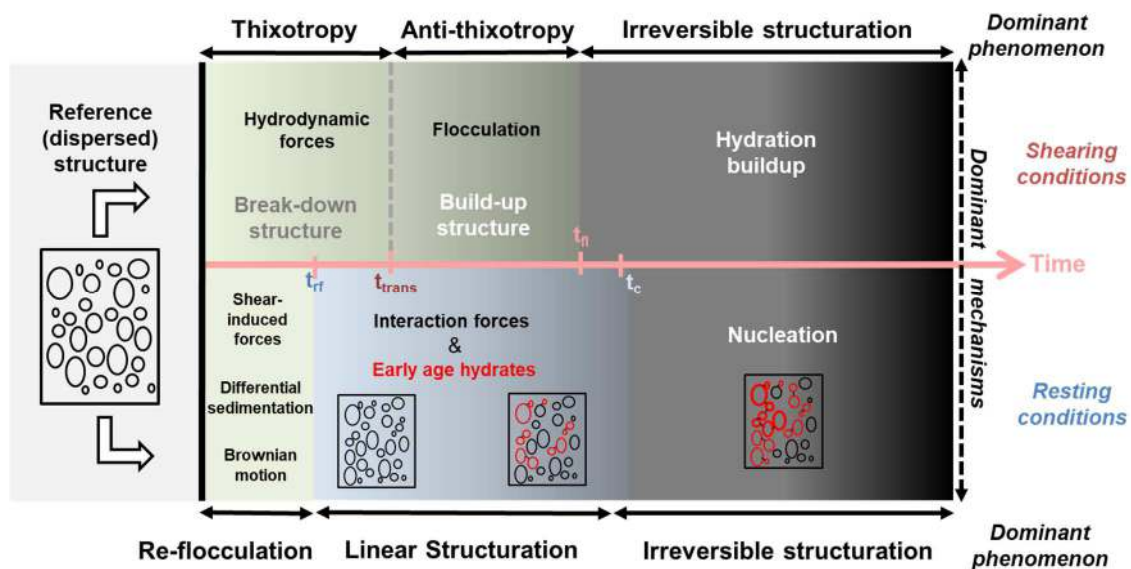
196 where $\tau_{s,floc}$ is the static yield stress resulted from the re-flocculation process (Pa) [37], A_{thix} is
 197 the structuration rate (Pa/min), and t_c' is the period over which non-linear structuration occurs.

198 ***b) Rigidification process***

199 The storage modulus (G') evolution is often used to assess the structural build-up of cement-
 200 based materials at rest. Small amplitude oscillatory shear (SAOS) is the most recommended non-
 201 destructive test method to follow up the rigidification process. Recently, Ma et al. [28] have
 202 proposed a model to evaluate the structural build-up behavior based on the time evolution of G' ,
 203 which can be expressed according to **Eq. (6)**.

$$204 \quad G'(t) = G'_{floc} + R \cdot t \quad (6)$$

205 where G'_{floc} is the storage modulus resulted from the re-flocculation process (Pa) and R is the
 206 rigidification rate (Pa/min). According to various studies [27–29,38], two rigidification kinetics
 207 can be observed at an early age, including a short-term flocculation that occurs within a few
 208 hundred seconds, as it is the case for the static yield stress, and then a long-term rigidification
 209 due to C-S-H nucleation and hydration. This evolution induces a larger number of pseudo-point
 210 contacts between flocculated particles at rest, leading to the formation of an interconnected
 211 percolation network reflected by a stabilized storage modulus, as stated in [29]. Accordingly, the
 212 different dominant mechanisms responsible for the time-dependent rheological behavior of
 213 cement-based materials are summarized in **Fig.2**.



214

215 **Fig. 2 :** Schematic of the physico-chemical mechanisms of the time-dependent behavior of
 216 cement-based materials during **shear** and **rest** conditions

217 ***c) Printing stability criteria***

218 The printed layer should be able to withstand its own weight. Besides, as subsequent layers are
 219 deposited, the bottom layers should be able to sustain gravity-induced stresses [1,8]. Considering
 220 the time evolution of the rheological behavior, the structuration rate should then be adjusted
 221 according to the height-rising rate of the printing process. Thus, in order to prevent collapsing,
 222 the static yield stress of the printed material should satisfy the strength-based stability condition
 223 given in equation **Eq. (7)**, as follows:

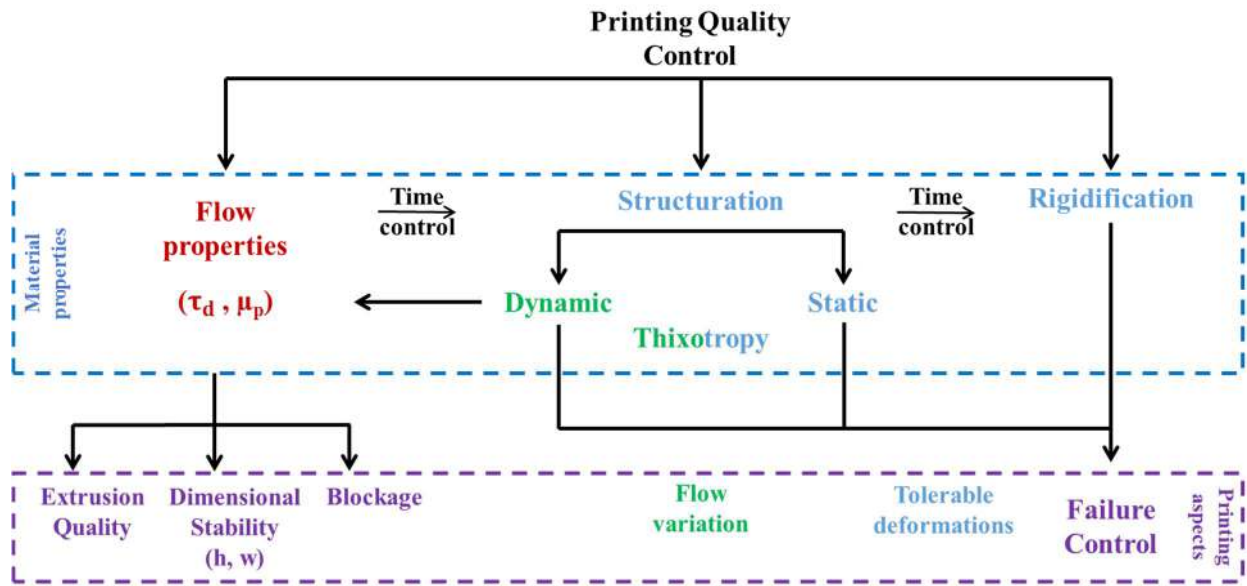
$$224 \quad \tau_s(t) > \rho g h(t) / \sqrt{3} \quad (7)$$

225 Although the gravity-induced layer stress may remain below the material yield stress, the
 226 resulting strain in the layer can compromise the dimensional stability of the printed element.
 227 Therefore, the strain of the printed layers should stay below a tolerable deformation γ_{lim} to
 228 prevent any dimensional instability. As a result, the rigidity of the printable material $G = \tau_s / \gamma_c$
 229 must be higher than $\rho g h(t) / \gamma_{lim}$ [8].

230 Furthermore, aside from the strength-based failure described above, the loss of stability or
 231 buckling seems to be also frequent in-print failure mode. Buckling failure generally occurs due
 232 to progressive lateral deformations. The eccentric layer displacement may also result in an
 233 unstable structure and stability failure. The failure due to buckling is mainly governed by the
 234 material properties such as the elastic modulus at a fresh state. Additionally, the geometry or
 235 slenderness of the printed structure may also affect the buckling failure. Other factors that can
 236 lead to bucking failure will be discussed later.

237 **2.3. Printing quality control**

238 Considering the time-dependent behavior of cement-based materials, it is crucial to control the
 239 quality of printing over time. The main aspects that should be considered are summarized in
 240 **Fig.3.**



241

242

243

Fig. 3 : Printing quality control by monitoring the time-dependent behavior of printable materials

244 a) Thixotropy index

245

246

247

248

249

250

251

252

In 3D printing applications, materials with a high rate of structuration are usually used to prevent plastic failure [8]. However, high structuration during pumping and extrusion phases may lead to material clogging and a decrease in the extrusion quality [39,40], thus hindering the stability of the printed structure [41]. It is therefore essential to take into consideration the increasing rate of the dynamic threshold, which can be useful to avoid these problems. In the present study, the area between the static and dynamic yield stress growths within the linear domain (**Fig. 4**) was used as a thixotropy index to evaluate the printability window of cement-based materials. This area can be expressed by the equation **Eq. (8)**.

253

$$\Phi_{\text{thix}} = \underbrace{(\tau_{s,\text{floc}} - \tau_{d,0}) \cdot t_c}_{(1)} + \underbrace{A_{\text{thix}} \cdot t_c^2 / 2}_{(2)} - \underbrace{\beta_{\text{thix}} \cdot t_c^2 / 2}_{(3)} = \Phi_0 + \Phi_{\text{struct}} \quad (8)$$

254

255

256

257

where the first term **(1)** represents the energy required to form the initial structure, the second term **(2)** refers to the storage energy due to static structuration, and the third term **(3)** is the energy loss due to dynamic structuration.

258

259

260

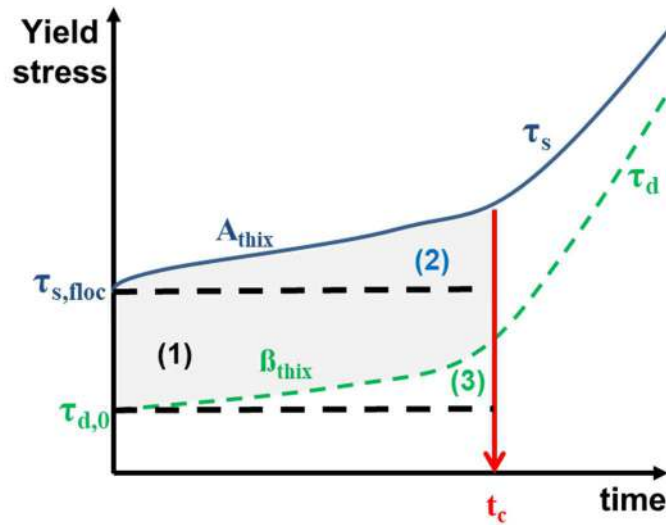
261

262

263

In the case of materials with low thixotropy, the structuration terms **(2)** and **(3)** can be neglected and the difference between the initial stress thresholds (Φ_0) becomes the dominant criterion for printability. On the other hand, for materials with a high degree of thixotropy, the structuration terms (Φ_{struct}) will be the dominant term to consider. This term takes into account not only the structuration rates of the material but also its open time t_c , during which the evolution of the material properties remains linear and reversible. These properties can be extremely limited for

264 some types of materials. It is also important to distinguish the different behaviors that can occur
 265 depending on the printing mode, which will be discussed in the following section.



266

267

Fig. 4: Thixotropic area used to define the printability window

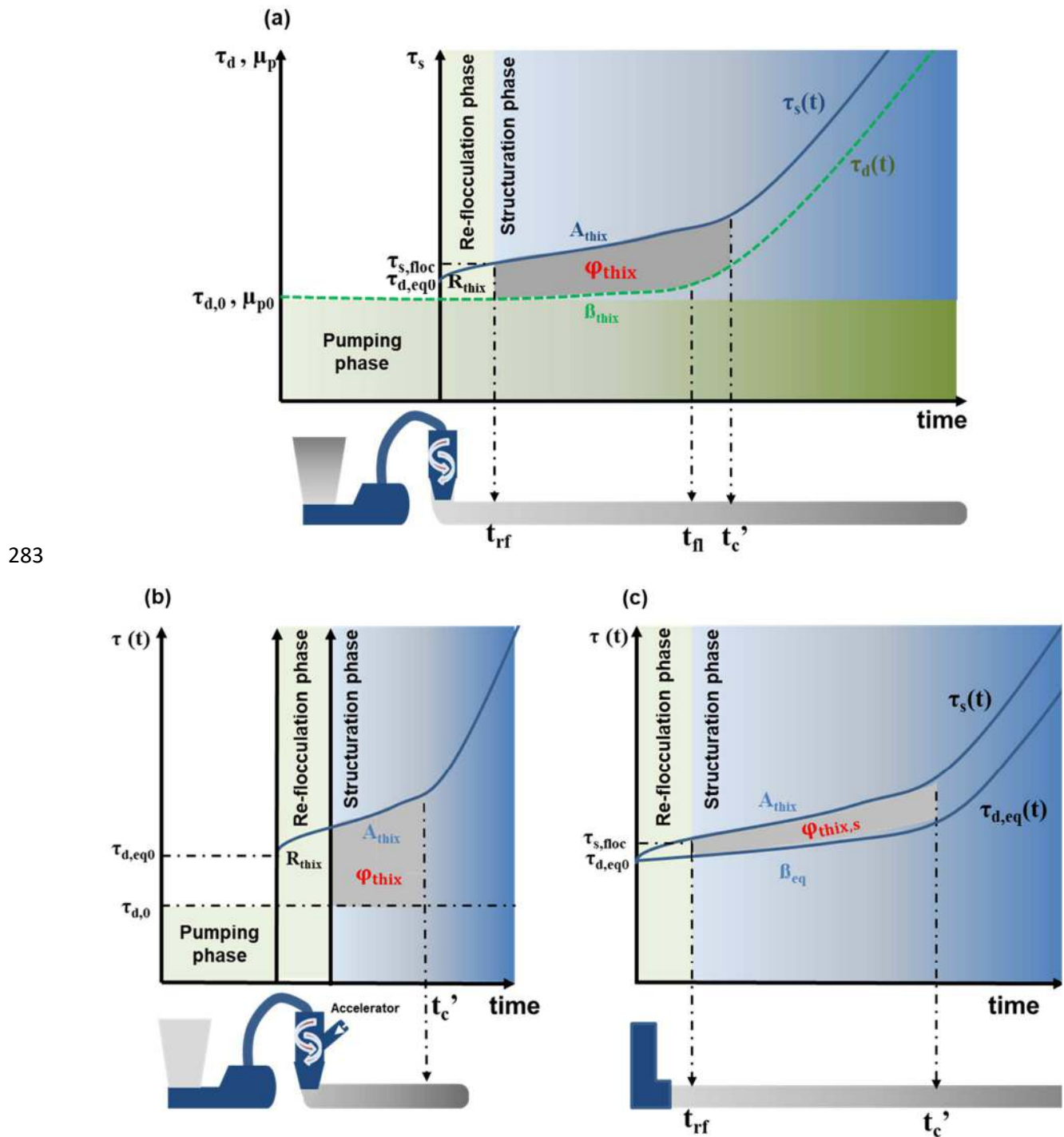
268 ***b) Printing mode cases***

269 As mentioned previously, the thixotropy index ϕ_{thix} allows evaluating the printability window
 270 of the material. Higher ϕ_{thix} values ensure a larger printability window. However, this index
 271 seems to be more adapted to continuous shear extrusion and free flow deposition printing
 272 processes, where the material is sheared during the extrusion phase. In the case of set-on-demand
 273 printing, in which the accelerators are injected at the nozzle level, the workability does not
 274 interfere with the buildability aspect of the material. In this case, the dynamic structuration rate
 275 β_{thix} can be neglected. In the case of infinite brick extrusion, the structure is less disturbed, as
 276 the material is not subjected to shear. Hence, pseudo-dynamic structuration β_{eq} can be
 277 considered instead, obtained from the evolution of $\tau_{d,eq}$ during the flow onset. The structural
 278 term ϕ_{struct} can then be expressed by **Eq. (9)**, as follows.

279

$$\phi_{struct,static} = (A_{thix} - \beta_{eq}) \cdot t_c^2 / 2 \quad (9)$$

280 Different representations of the thixotropy index according to the considered printing mode
 281 processes are summarized in **Fig. 5**. In this study, only the continuous shear extrusion and free
 282 flow deposition will be investigated.



283

284

285 **Fig. 5 :** Thixotropic indices for different extrusion-based printing processes, including (a) free
 286 flow deposition, (b) set-on-demand printing, and (c) infinite brick extrusion

287 3. Materials and Test Methods

288 3.1. Materials and sample preparation

289 The investigated mixtures were proportioned using fine sand, general use Portland cement CEM
 290 I 52.5, and a modified polycarboxylate-based superplasticizer (SP). Supplementary cementitious
 291 materials (SCM) were used to reduce the amount of cement and improve the stability and the
 292 packing properties of the mixtures [37]. A viscosity modifying agent (VMA) has been
 293 incorporated in some mixtures to improve the rheology of printable mixtures. The mix designs
 294 were optimized based on a previous study [37]. The chemical and physical properties of the
 295 cementitious materials are summarized in **Table 3**. On the other hand, the proportions of the
 296 investigated mixture are presented in **Table 4**.

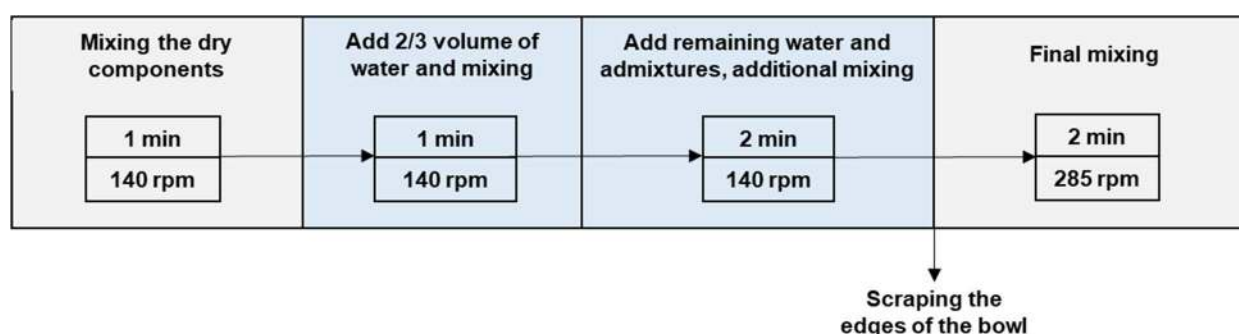
297 The mixtures were mixed in 2-liter batches using a standard Hobart mixer. The mixing method
 298 shown in **Fig. 6** was adopted to ensure efficient mixing, a similar dispersion state, and shear
 299 history.

300 **Table 3:** Physical and chemical properties of cementitious materials

	Chemical components (%)								Density (g/cm ³)	Fineness (m ² /kg)
	SiO ₂	Al ₂ O ₃	Fe ₂ O ₃	CaO	MgO	SO ₃	Na ₂ O eq.	ZrO ₂		
Cement	19.6	4.5	2.3	63.7	3.9	2.6	0.13	-	3.14	390
Silica fume	93.5	3.5	0.15	0.02	< 0.02	0.006	0.1	2.4	2.60	12 000
Fly ash (Class F)	52.5	22.5	8.5	3.5	3	0.37	2.96	-	2.24	230
Limestone filler	0.9	-	-	97.8	-	-	-	-	2.71	426

301 **Table 4:** Proportions of the investigated mortar mixtures

	Fine sand (kg/m ³)	CEM 1 (kg/m ³)	Silica fume (kg/m ³)	Fly ash (kg/m ³)	Limestone filler (kg/m ³)	Water (kg/m ³)	SP (% woc)	VMA (% woc)
MFA	981	649	93	185	-	260	1.2	-
MFA-V	981	649	93	185	-	260	1.2	0.5
MLF	981	649	93	-	223	260	1.2	-
MLF-V	981	649	93	-	223	260	1.2	0.5



302

303 **Fig. 6:** Mixing procedure for the investigated mortar mixtures

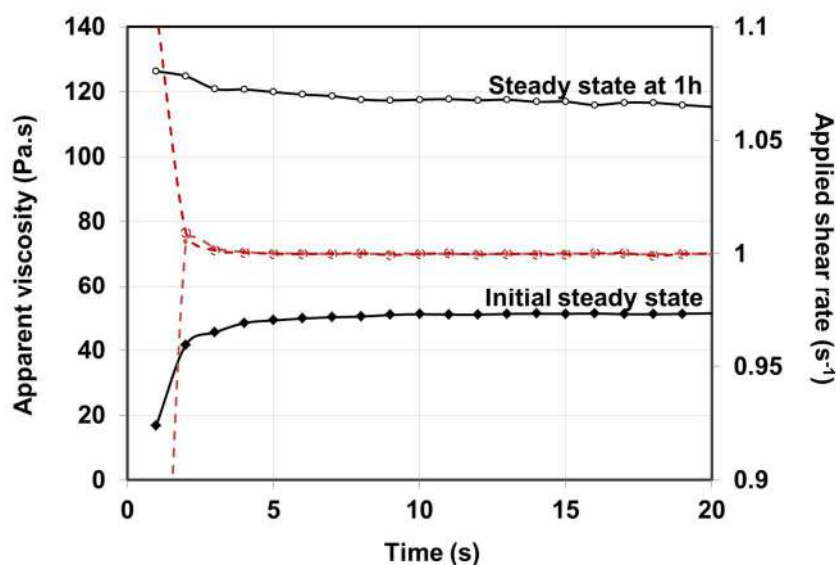
304 3.2. Rheological measurements

305 Rheological measurements were performed using a Discovery Hybrid Rheometer 2 (DHR2)
 306 equipped with a 4-blade vane geometry to prevent wall slippage [42]. The cup and bob diameters
 307 are 30.36 mm and 26.198 mm, respectively. The shear gap size was set at 4 mm. The
 308 temperature was kept constant at $20 \pm 0.1^\circ\text{C}$. A dispersion reference state was fixed for all the
 309 mixtures through a pre-shear period of 120 s at 200 s^{-1} [43].

310 a) Hysteresis loop

311 First, the hysteresis loop protocol was used to investigate the time-dependent flow behavior of
 312 the investigated mixtures and reproduce the pumping conditions during printing. Step-wise shear
 313 rates were applied from 1 s^{-1} to 200 s^{-1} , followed by downward ramps. Each ramp was
 314 maintained for a maximum of 20 s, which corresponds to the time needed for the mixtures to
 315 reach a steady state at 1 s^{-1} , as shown in **Fig. 7**. As a means of optimizing the time measurement,
 316 an equilibrium condition was imposed on the deviation tolerance of apparent viscosity under a
 317 constant shear rate, set at 0.01%. This procedure was repeated for the first two hours, with a 20-
 318 second rest period between each test, as shown in **Fig. 8**. The modified Bingham model was used
 319 to determine the dynamic yield stress and plastic viscosity using the descending curve, according
 320 to **Eq. (10)** [44] :

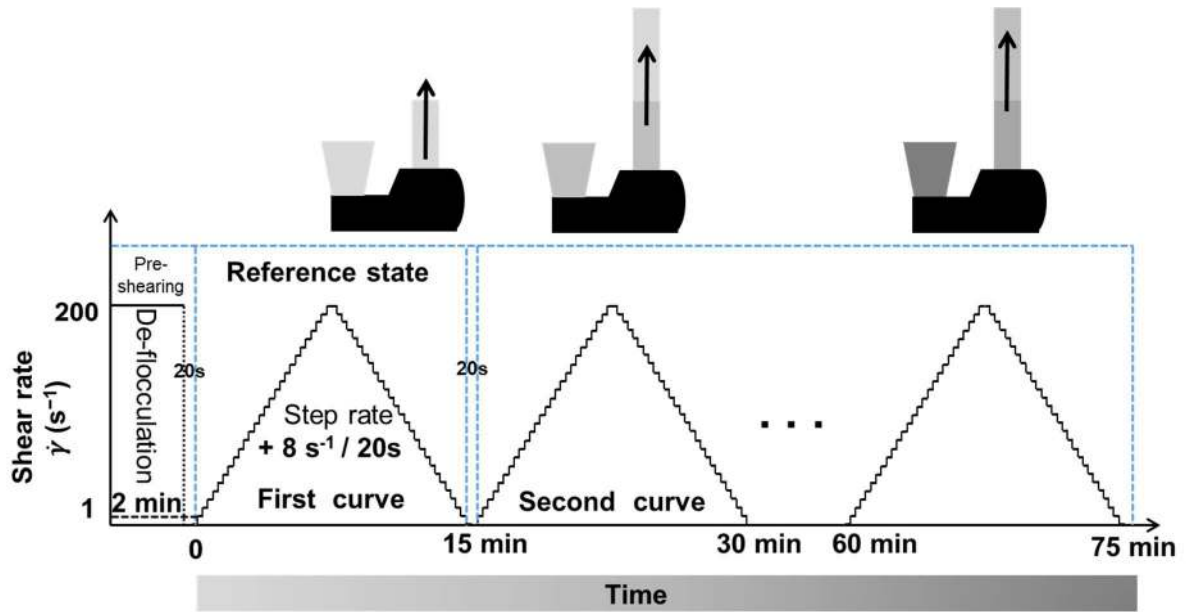
$$321 \quad \tau(\dot{\gamma}) = \tau_d + \mu_p \dot{\gamma} + c\dot{\gamma}^2 \quad (10)$$



322

323

Fig. 7: Steady state curves at different ages



324

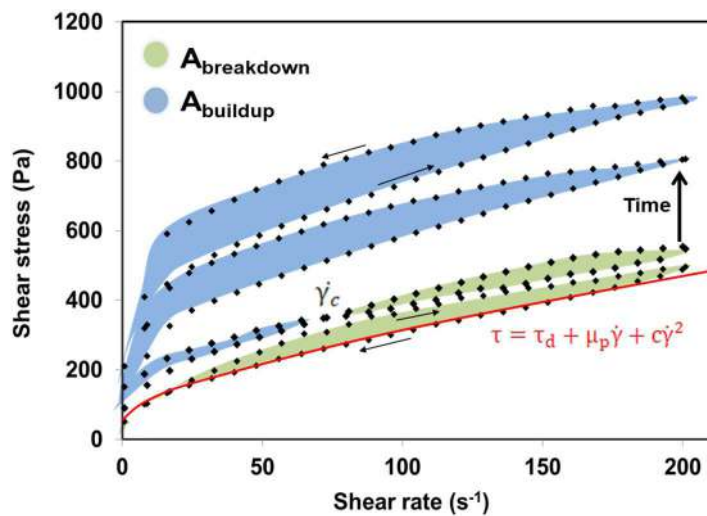
325

Fig. 8: Hysteresis loop protocols

326 During flow measurements, a competition between flocculation and dispersion occurs, hence
 327 changing the shape of the loops over time. This will be monitored to evaluate the flow changes
 328 that may occur during pumping and extrusion. The area between the upward and downward flow
 329 curves was determined and used to assess the rates of structural breakdown and build-up of the
 330 investigated mixtures, according to **Eq. (11)**.

$$331 \quad R_{\text{buildup}} = \frac{|A_{\text{buildup}}|}{|A_{\text{buildup}}| + |A_{\text{breakdown}}|} \quad \text{and} \quad R_{\text{breakdown}} = 1 - R_{\text{buildup}} \quad (11)$$

332 where $A_{\text{breakdown}}$ represents the area where the up-flow curves are greater than the down-flow
 333 curves and A_{buildup} is the reverse-case area. The crossover shear rate $\dot{\gamma}_c$ has been determined as
 334 shown in **Fig. 9**.



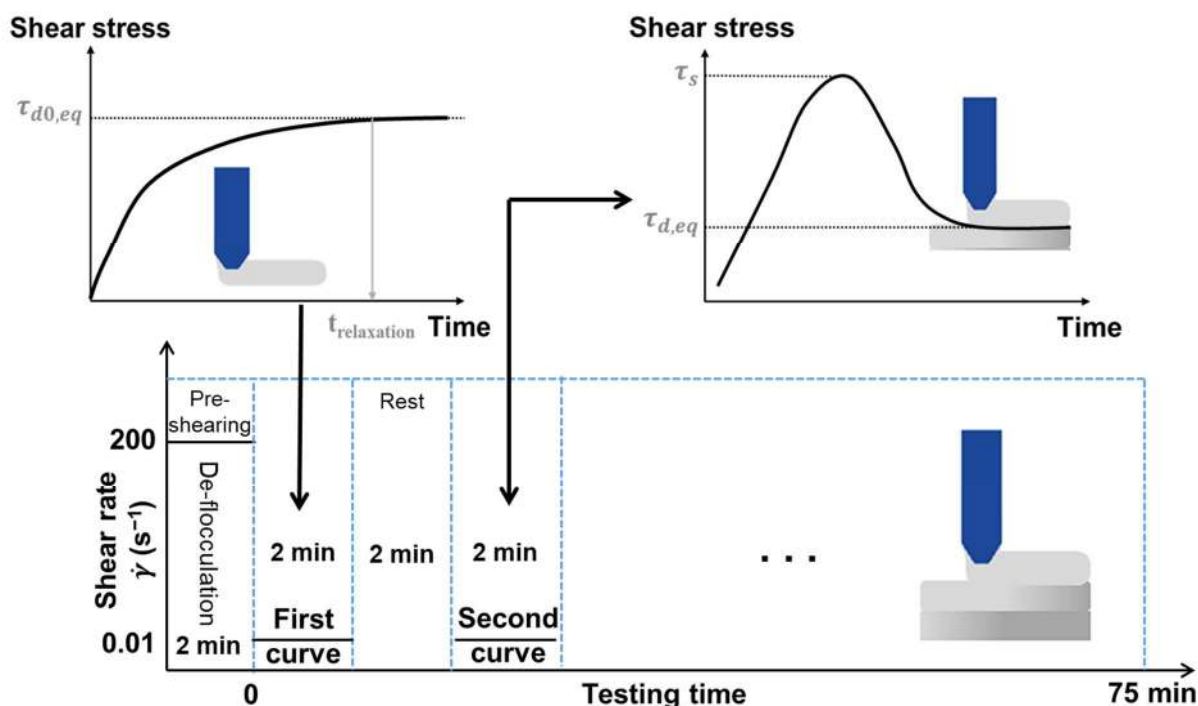
335

336

337

Fig. 9: Hysteresis loop areas depending on the flow curve direction338 **b) Yield stress growth**

339 Once the material flows out of the nozzle, it starts to restore its structure at rest, which evolves
 340 with time. In order to monitor the evolution of this structuration after extrusion, the material is
 341 subjected to a low shear rate of 0.01 s^{-1} immediately after the pre-shearing. This low shearing is
 342 repeated every 2-minute, as shown in **Fig. 10**. The static yield stress τ_s refers to the peak value of
 343 the flow onset curve, while the equilibrium stress refers to the dynamic yield stress $\tau_{d,eq}$ of
 344 partially de-structured network, as explained in **section 2**. In order to assess the buildability of
 345 the investigated mixtures, the growth of yield stress has been assessed and fitted with the models
 346 given in **Eqs. (4) and (5)**.



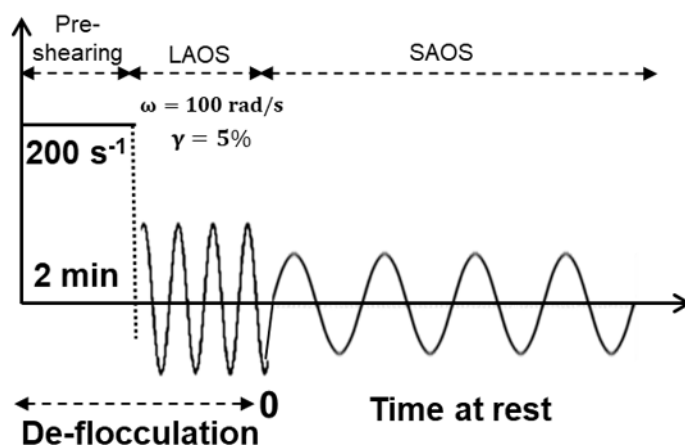
347

348

Fig. 10: Measurement protocol of the stress growth349 **c) SAOS measurements**

350 Small amplitude oscillatory shear (SAOS) tests were used to capture the evolution of the
 351 structural build-up of the investigated mixtures. These tests were carried out at shear strain
 352 of 10^{-5} , which is within the linear viscoelastic domain of the mixtures to avoid breaking their
 353 microstructure, and an angular frequency of 10 rad/s [27]. The tested samples were first pre-
 354 sheared at a constant shear rate of 200 s^{-1} for 2 minutes and then subjected to a large amplitude

355 oscillatory shear (LAOS) at a shear strain of 5% and an angular frequency of 100 rad/s for 10 s
 356 to achieve good dispersion [45], as shown in **Fig. 11**.



357

358

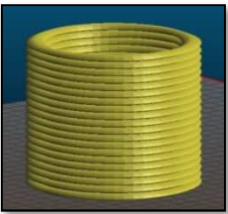
Fig. 11: SAOS measurement protocol [27]

359 3.3. Printing trials

360 Printing trials were conducted at different ages to evaluate visually the changes in printing
 361 quality over time. The first trial was performed **15 min** after mixing, the second after **30 min**,
 362 and the third one after **45 minutes** of age. Circular hollow columns of 100 mm diameter and 10
 363 mm width were printed until their collapse. The structural evolution of the investigated mixtures
 364 was compared with the vertical building rate of the printed layers. The printing parameters are
 365 summarized in **Table 5**. All samples were printed at a controlled room temperature of 20 ± 1 °C.

366

Table 5: Printing parameters

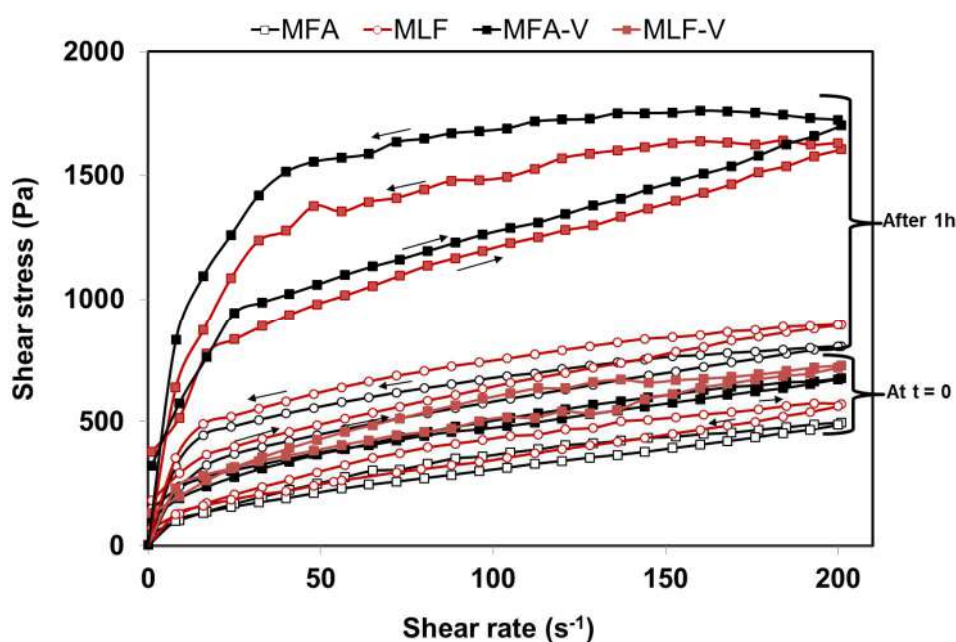
Input sliced model	Height of single layer	Printing velocity	Type of nozzle	Extrusion device	Feeding rate
	5 mm	20 mm/s	Circular (Ø10 mm)	Ram & screw extruder	275.71 mm ³ /s

367 4. Results and discussions

368 4.1. Time-dependent behavior during flow

369 The hysteresis loops of the investigated mixtures are summarized in **Table 6** and **Fig. 12**. The
 370 hysteresis loops and flow parameters (τ_d , μ_p) increase with time. This is more pronounced for

371 mixtures containing VMA. The mixtures MFA-V and MLF-V exhibited higher build-up
 372 compared to those made without VMA, and the minimum shear rate values required to destroy
 373 the formed network were higher compared to other mixtures. This can be due to water adsorption
 374 on the long chain polymers of the VMA via hydrogen and ionic bonds, thus resulting in higher
 375 cohesiveness, which requires higher energy to break down the formed flocs [46]. A transitional
 376 time of 25 minutes was observed between the two mechanisms for the MFA-V and MLF-V
 377 mixtures, compared to 65 minutes for the mixtures without VMA, as shown in **Fig. 13**. This time
 378 defines the period during which some of the formed flocs can no longer be broken down under
 379 the provided shearing energy. During this period, the viscosity increases progressively due to the
 380 friction between the undestroyed flocs and suspended particles, leading to a shear-thickening
 381 behavior. During printing, this can cause unstable mixes, which may compromise their
 382 pumpability and extrusion quality [47]. The competition between structural break-down due to
 383 hydrodynamic forces and structural build-up due to collisions induced by flocculation
 384 mechanisms is the driving force behind microstructural changes in cement-based materials [48].
 385 The Brownian motion induces the particles to move to the most favorable positions in terms of
 386 structure-entropy.



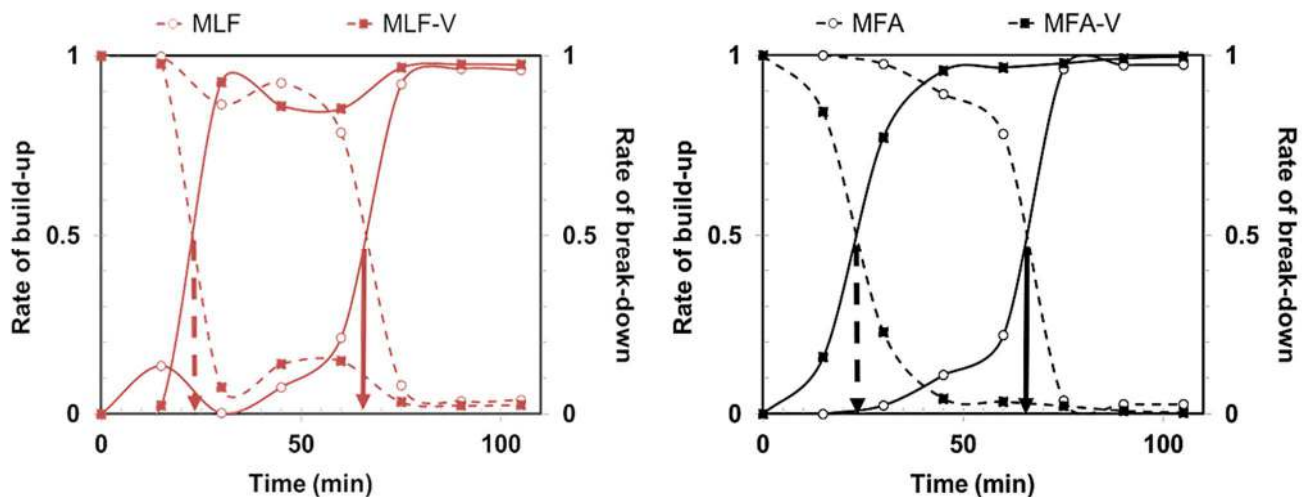
387
 388 **Fig. 12:** Hysteresis loop curves of the tested mixtures at $t=0$ and **1h** of measurement

389 Moreover, the mixtures containing limestone filler exhibited variable breakdown and build-up
 390 competition over time (**Fig. 13**). This can be explained by the unstable structure formed by
 391 limestone aggregates [47]. This is related to the effects of the Ostwald ripening phenomenon due
 392 to the dissolution and precipitation of CaCO_3 particles [27,49]. This can result in decreasing the

393 crossover shear rate for MLF and MLF-V mixtures during the initial phase and increasing their
 394 structural breakdown compared to MFA and MFA-V mixtures.

395 **Table 6:** Flow parameters and hysteresis areas of the investigated mixtures

	Time (min)	τ_d (Pa)	μ_p (Pa.s)	$ c $	R^2	A_{buildup} (Pa/s)	$A_{\text{breakdown}}$ (Pa/s)	$\dot{\gamma}_c$ (s ⁻¹)
MFA	15	70	2.86	0.0044	0.98	0	8 279	-
	30	87	2.90	0.0050	0.97	-134	5 552	6.5
	45	108	3.09	0.0058	0.95	-451	3 719	18.6
	60	143	3.26	0.0071	0.91	-1 306	4 661	47.9
	75	185	4.86	0.0132	0.91	-9 356	361	-
	90	254	6.36	0.0191	0.88	-15 002	422	-
	105	338	7.93	0.0251	0.85	-18 188	500	-
MFA - V	15	161	4.21	0.0091	0.94	-782	4 177	21.8
	30	202	5.00	0.0128	0.91	-3 930	1 161	-
	45	258	6.42	0.019	0.88	-11 570	519	-
	60	337	8.14	0.0253	0.86	-17 934	631	-
	75	456	11.52	0.0393	0.83	-36 176	816	-
	90	691	17.15	0.0637	0.78	-66 014	554	-
	105	1 068	28.28	0.1085	0.80	-119 869	404	-
MLF	15	89	3.06	0.0041	0.98	-2 157	13 897	35.0
	30	103	3.09	0.0042	0.97	-18	6 793	1.0
	45	117	3.54	0.0070	0.96	-356	4 390	8.50
	60	166	3.21	0.0051	0.91	-1 282	4 733	30.09
	75	213	4.82	0.0122	0.90	-6 450	556	-
	90	279	7.03	0.0210	0.89	-16 782	626	-
	105	354	8.62	0.0268	0.86	-18 880	776	-
MLF - V	15	242	2.83	0.0025	0.99	-272	11 361	29.43
	30	310	3.81	0.0069	0.99	-7 249	577	188.07
	45	367	4.26	0.0085	0.98	-5 505	895	184.28
	60	463	4.27	0.0085	0.98	-6 309	1 089	144.63
	75	634	6.48	0.0192	0.94	-31 494	1 074	-
	90	781	11.20	0.0362	0.91	-47 452	1 147	-
	105	1357	31.39	0.1217	0.90	-75 616	1 920	-



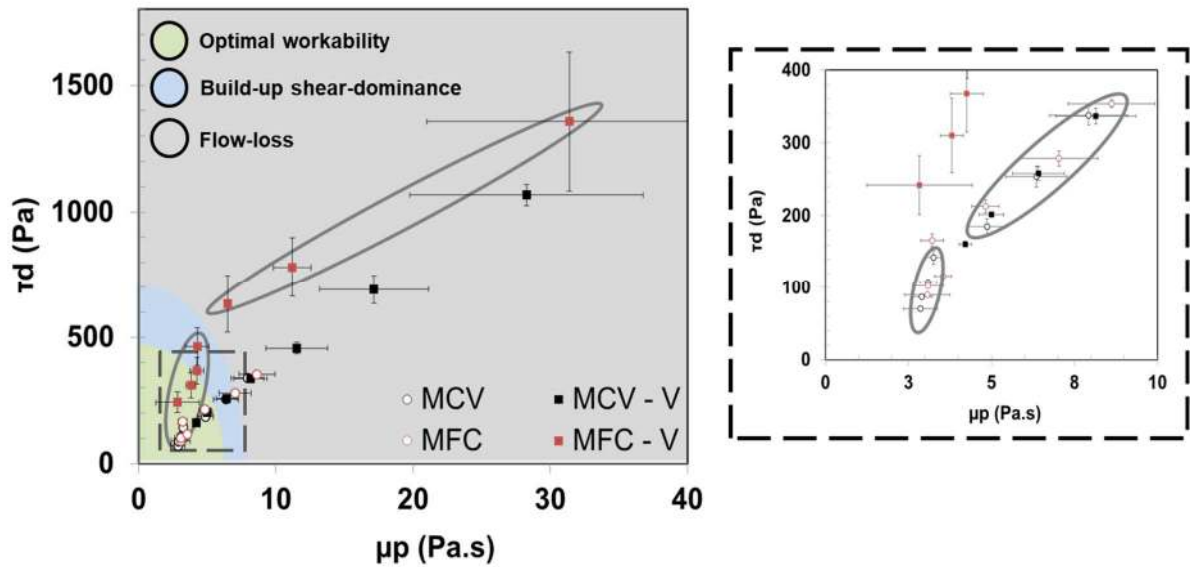
396

397 **Fig. 13:** Competition between the breakdown (**dashed line**) and the build-up (**bold line**)
 398 structuration of the mixtures with time

399 Accordingly, the time-dependent flow behavior is highly dependent on mixture composition. As
 400 shown in **Fig. 14**, a two-stage evolution of the flow behavior can be observed. In the first stage,
 401 the dynamic yield stress increases due to structural build-up, while the plastic viscosity varies
 402 slightly. In the second stage, the plastic viscosity drastically increases, marking the beginning of
 403 the flow loss. In order to prevent any blockage during the printing process, it is crucial to control
 404 the first evolution phase of the flow properties. This is mainly driven by the evolution of the
 405 dynamic threshold.

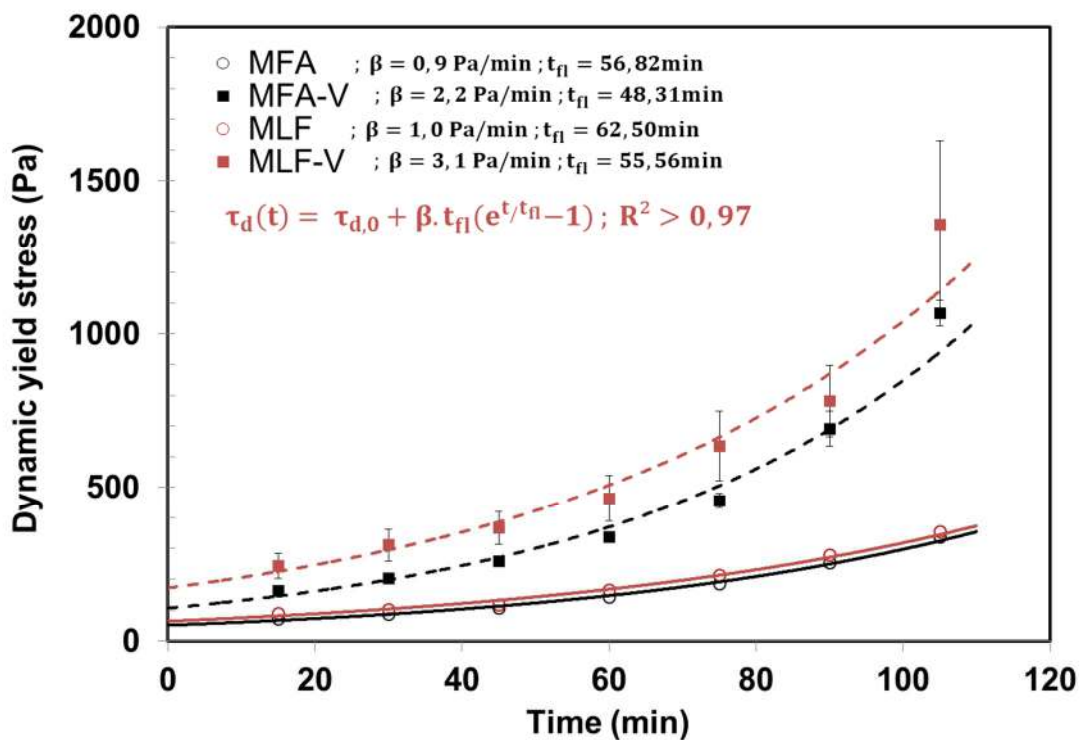
406 As can be observed in **Fig. 15**, the proposed model in **Eq. (1)** is shown to adequately describe the
 407 time evolution of dynamic yield stress. Mixtures containing VMA are found to have a shorter
 408 workability period and higher dynamic structuration kinetics than the other mixtures.

409 It is important to mention that the time of the workability loss (t_{fl}) may not match the transitional
 410 time between the break-down and build-up phases. Indeed, the t_{fl} marks the beginning of the
 411 irreversible structuration due to hydration, while the transitional time indicates the balance
 412 between formed and destroyed flocs, which mainly depends on the shearing energy.



413
414

Fig. 14: Time evolution of flow properties of the investigated mixtures



415

416 Fig. 15: Comparison between the experimental dynamic yield stress values and fitted model

417 4.2. Time-dependent behavior at rest

418 The various stages of the structural build-up of the mixtures were characterized by the time
419 evolution of both the static yield stress and storage modulus.

420 The stress growth curves during different structuration phases are shown in **Fig.A1** in **Appendix**
421 **A**. As mentioned earlier in **section 2**, Brownian motion, shear-induced forces, and differential

422 sedimentation will result in re-flocculation of the particles, hence resulting in a microstructural
423 rebuild after shearing. This process will last a few hundred seconds until the interparticle forces
424 reach equilibrium but can take a longer time in the case of mixtures containing VMA due to its
425 high molecular weight (**green curves**). Once the interparticle forces reach equilibrium, the
426 thixotropic structure rapidly regains stiffness due to an increase in viscosity. Then, the static
427 yield stress starts to increase due to the agglomeration of cement particles caused by colloidal
428 interactions and nucleation of early hydration products at their contact points (**blue curves**). A
429 network of percolation paths is then formed with significant strength (**red curves**).

430 According to the results presented in **Table 7**, the addition of VMA resulted in a higher effect on
431 the re-flocculation kinetics R_{thix} than the structuration rate A_{thix} . The presence of VMA polymers
432 induces bridging forces which promote the flocculation of the system and rapidly build up its
433 yield stress at rest [50,51]. Moreover, it seems that the addition of the VMA delays the critical
434 time between the linear and non-linear regimes, which can be correlated with the setting time.
435 Similar results have also been reported in the literature [52–54]. However, under shear, the
436 critical time t_{fl} decreased in the case of mixtures containing VMA. This may be related to the
437 effect of the shear stress on the long-chain polymer solutions which promotes molecular
438 crosslinking and thus increases the dynamic structuration kinetics [53].

439 Moreover, the investigated mixtures displayed comparable rates of structuration A_{thix} even
440 though their thixotropic behavior is quite different considering the B_{thix} parameter. The use of
441 $\varphi_{thix,s}$ index resulted in different classifications of the investigated mixtures based on their
442 thixotropy. For example, the mixture MFA-V is more thixotropic than MFA, which is not the
443 case when the φ_{thix} index is used for classification. The classification based on the latter index is
444 more reliable because it considers the thixotropy in both flocculation and de-flocculation states,
445 whereas the classification based on $\varphi_{thix,s}$ does not.

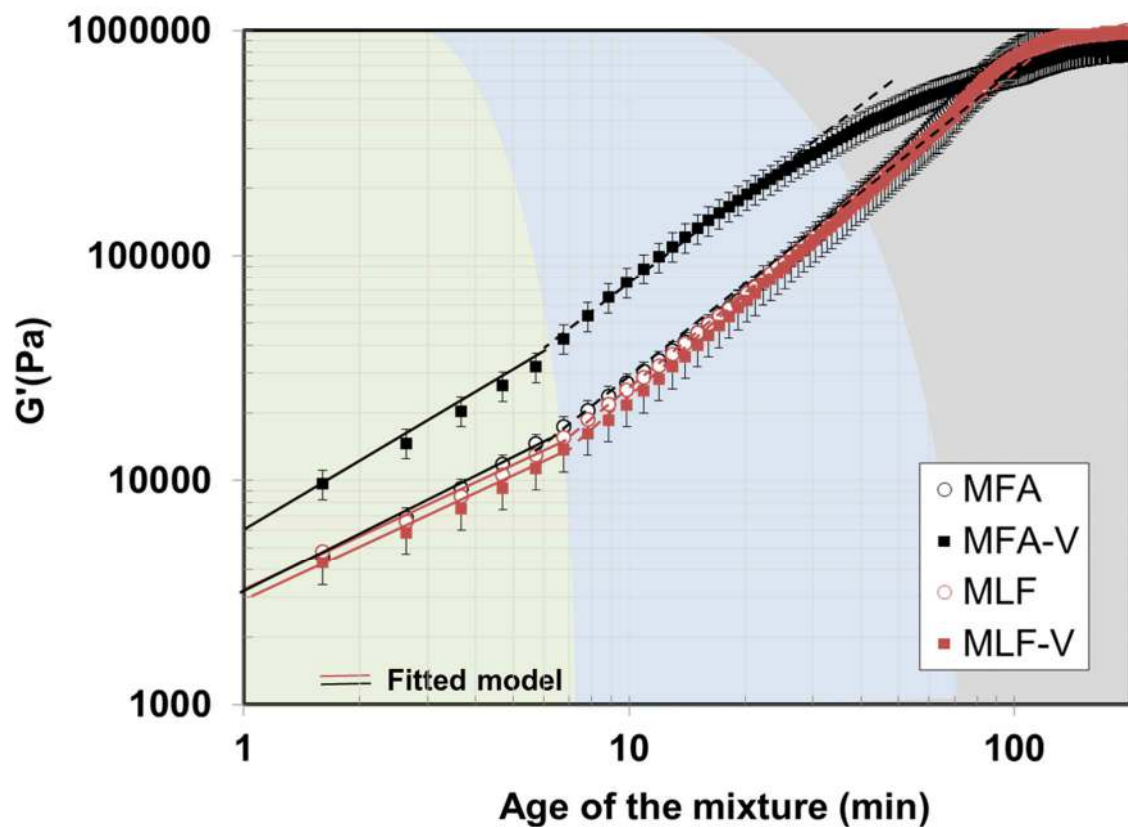
446 The different phases of rigidification based on the storage modulus evolution are presented in
447 **Fig. 16**. On the other hand, the established model parameters are summarized in **Table 8**. Good
448 fitting with the proposed model suggests that there exist two distinct kinetics of rigidification. At
449 an early age, first, the structure evolves due to particle re-flocculation and then increases linearly
450 due to the formation of successive paths of interconnected flocs until it reaches a stabilized
451 structure. These results are consistent with those reported in the literature [27–29].

452 The incorporation of VMA resulted in an increased rigidification rate (R) of the mixture MFA,
453 but surprisingly without a significant effect in the case of the MLF mixture. This result was in

454 line with the $\Phi_{\text{struct-static}}$ values, reflecting the static structural-build-up factor during yielding.
 455 Thus, the rate of rigidification is a good indicator of the build-up kinetics of the mixtures at rest.
 456 The mixtures MFA, MLF, and MLF-V developed their rigidity in a similar manner. This is an
 457 indication that these mixtures may have similar build-up behaviors. Similar results were also
 458 reported in the literature, where different mixtures resulted in comparable rates of rigidification
 459 [48,55]. However, the mixtures containing limestone filler exhibited a more rigid structure
 460 during the nucleation phase. This can be due to the physical and chemical effects of the
 461 limestone filler, allowing more nucleation sites for cement particles [56].
 462 It should be noted that the structuration kinetic derived from the stress growth results differs
 463 from the rigidification kinetic. Some mixtures can quickly develop their percolated structure
 464 without exhibiting a higher strength [57], as shown in **Fig. 17**. Besides, G' evaluated at a strain of
 465 0,001% mainly reflects the strength of C-S-H bridges between cement particles. Hence,
 466 imposing large strains during the static yield stress measurements (total strain for the
 467 measurement at a shear rate of 0.01 s^{-1} is 1.2, which is much larger than 10^{-5}), causes significant
 468 destruction of C-S-H networks, which may not be considered during the static yield stress
 469 measurements [28,58].

470 **Table 7:** Summary of the structuration rate parameters of the investigated mixtures

	MFA	MFA - V	MLF	MLF - V
$\tau_{s, \text{floc}}$ (Pa)	282	323	140	200
R_{thix} (Pa/min)	21	22	20	30
A_{thix} (Pa/min)	3.6	3.5	2.8	2.9
t_c' (min)	81.30	113.64	78.74	90.91
β_{eq} (Pa/min)	2.9	2.7	1.9	2.3
R^2	0.995	0.977	0.976	0.969
$\Phi_{\text{struct-static}}$ (Pa.min)	2313	5165	2573	2648
$\varphi_{\text{thix,s}}$ (Pa.min)	19 549	23 613	6568	1199
β_{thix} (Pa/min)	0.9	2.2	1.0	3.1
t_{fl} (min)	56.82	48.31	62.50	55.56
Φ_{struct} (Pa.min)	4358	1529	3359	-278
φ_{thix} (Pa.min)	16 404	9371	6531	2629



471

472 **Fig. 16 :** Time evolution of the storage modulus – **Green:** Re-flocculation phase, **Blue:** Linear
 473 rigidification, and **grey:** Nucleation phase.

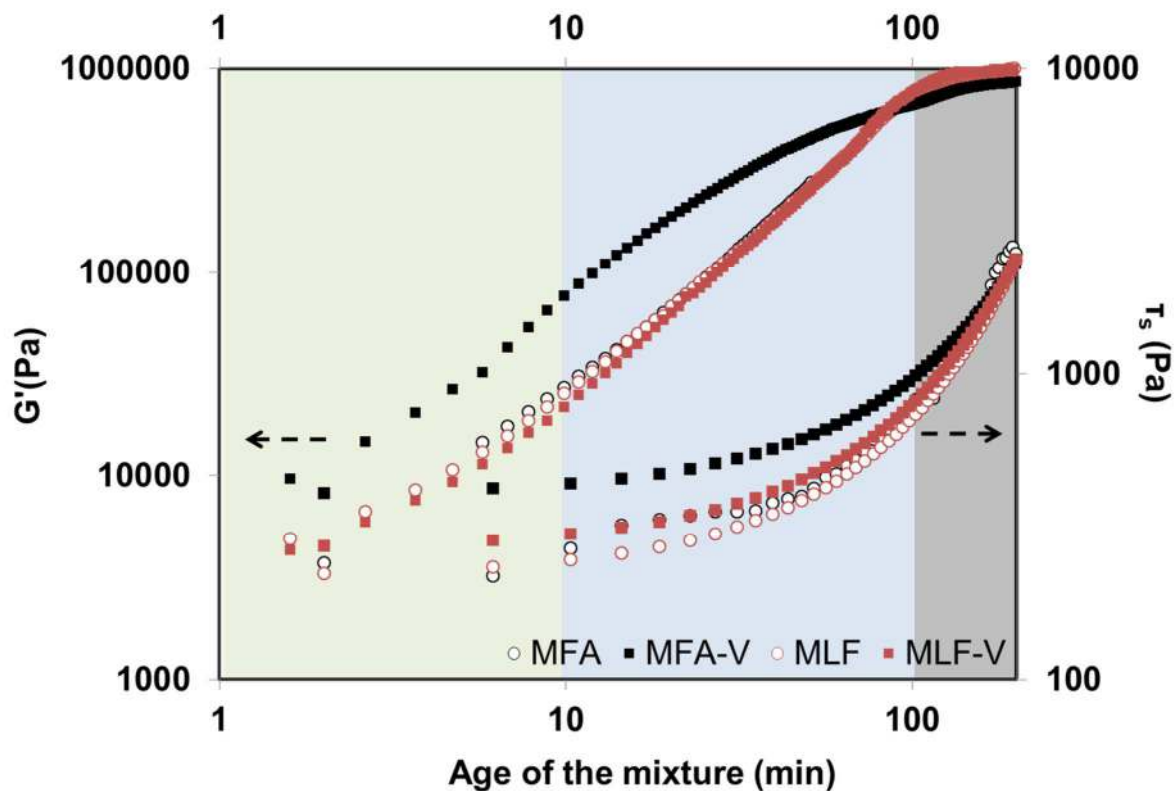
474

475

Table 8 : Rigidification parameters of the investigated mixtures

	G'_0 (Pa)	R (Pa/min)	R^2	G'_{floc}
MFA	1604	5 407	0.975	45 276
MFA-V	2489	9 481	0.997	53 768
MLF	1593	5 258	0.977	45 290
MLF-V	1435	5 166	0.976	44 056

476



477
478 **Fig. 17** : Storage modulus vs. Static yield stress evolution

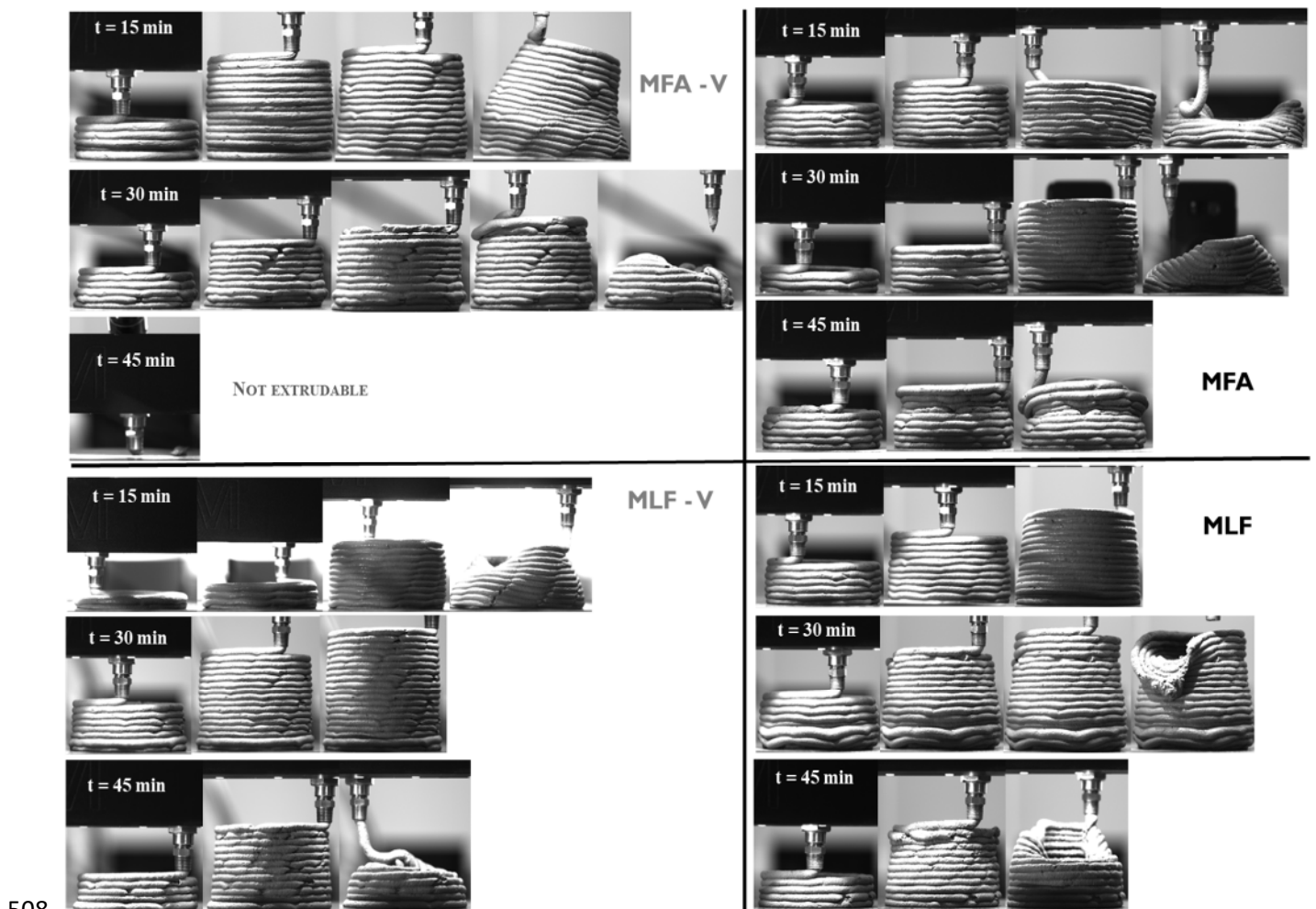
479 **4.3. Quality control of printing through time-dependent rheological behavior**

480 The results of the printing tests are shown in **Fig. 18**. It can be seen that the printing quality is
481 highly affected by the time-dependent behavior of mixtures. It is important to mention that the
482 investigated mixtures exhibited similar initial extrudability performance evaluated by the
483 continuity of the filaments and the homogeneity of the layer's width. This can be due to their
484 comparable (R_{thix} , G'_{floc}) values. However, beyond t_n , the mixtures can no longer be printed due
485 to the workability loss. At a time relatively close to t_n , the extrusion quality of the mixtures
486 dropped. This was reflected by the discontinuity of the filaments and the decrease in their widths.
487 The pressure required to extrude the mixtures also increased, as shown in **Table 9**. This implies
488 an increase in the flow parameters (μ_p , τ_d), which is consistent with the results presented in the
489 previous section.

490 The buckling of the structure resulted in failure after a certain age. As a result, the strength-based
491 stability condition (**Eq. (7)**) failed to predict the layer of failure. However, good results have
492 been obtained during the initial tests, as shown in **Fig. 19**. It is noteworthy to mention that failure
493 for mixtures containing VMA observed after **15 min** was delayed due to the strong bond
494 between the layers, which prevents the transmission of the cumulative weight to the bottom,
495 causing a combined plastic-buckling failure. In addition, as the tolerable deformation values

496 decrease with time (**Fig. 20**), the printed element may experience brittle failure. A slight increase
 497 in tolerable deformations was observed in mixtures containing limestone filler. This can be due
 498 to the unstable structure discussed earlier.

499 Furthermore, a flow variation during printing was observed for some mixtures. This seems to
 500 occur when the dynamic yield stress increases during printing, as shown in **Fig. 21**. Since the
 501 extrusion pressure has been chosen for a lower flow threshold, an underflow layer is extruded,
 502 which generates instability in the printed structure, referring to MFA-V **30min** and MFA **45min**,
 503 as shown in **Fig. 18**. Moreover, when the transitional time t_{trans} between the dominant structural
 504 break-down and the structural dominant build-up is exceeded, another problem arises. The
 505 thickness of the layers is reduced, which may be due to the loss of shear efficiency at the nozzle
 506 level. This leads to the failure of the printed structure (see MFA-V **30min**, MFA and MLF
 507 **45min** in **Fig. 18**).



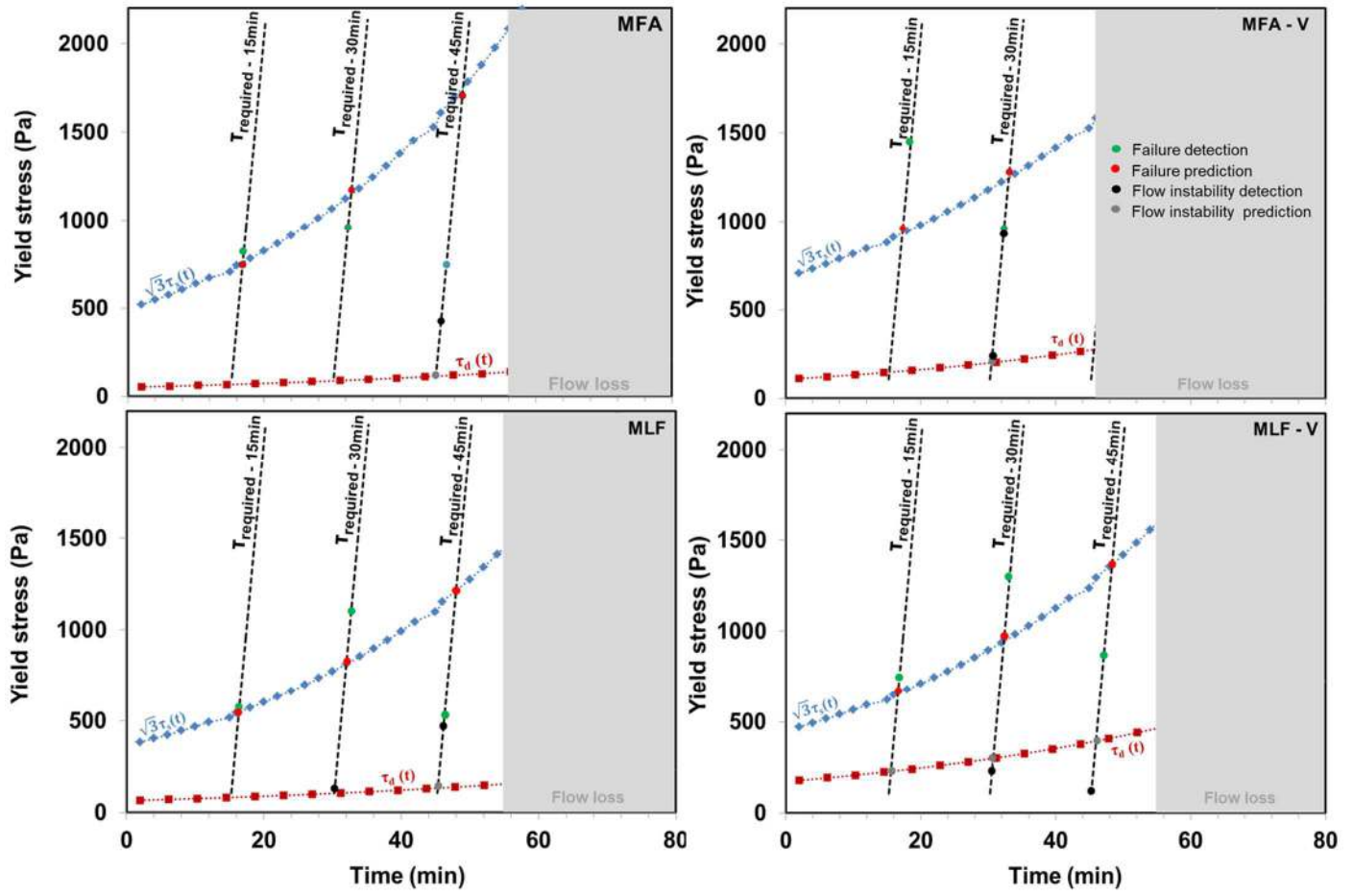
508

509 **Fig. 18** : Printing column at **15, 30, and 45** min of age of mixtures

510 To summarize, different types of failure can take place depending on the time of printing and the
 511 degree of thixotropy of each mixture (**Fig. 21**). Plastic failure occurred at an early age in
 512 mixtures with a low degree of structuration $\Phi_{\text{struct-static}}$. However, combined failure or buckling
 513 can occur due to geometric instability for more thixotropic mixtures. Additionally, flow
 514 instability may also lead to other failure modes. This is reflected by the width variation of the
 515 printed layer. When shearing efficiency decreases at the nozzle level due to dynamic
 516 structuration (β_{thix}), layer width decreases leading to an unstable structure. Two parameters must
 517 then be considered to prevent failure (t_{trans} , $\dot{\gamma}_c$). The critical shear rate $\dot{\gamma}_c$ must be higher than the
 518 nozzle rotational shear rate. Also, the pumping/extrusion pressure must be adjusted if the
 519 printing time exceeds t_{trans} . Another case can occur during multi-batch printing, resulting in an
 520 increase in the thickness of the freshly printed layer compared to the last layer underneath, which
 521 is beyond the scope of this paper.

522 **Table 9** : Summary of the printing results

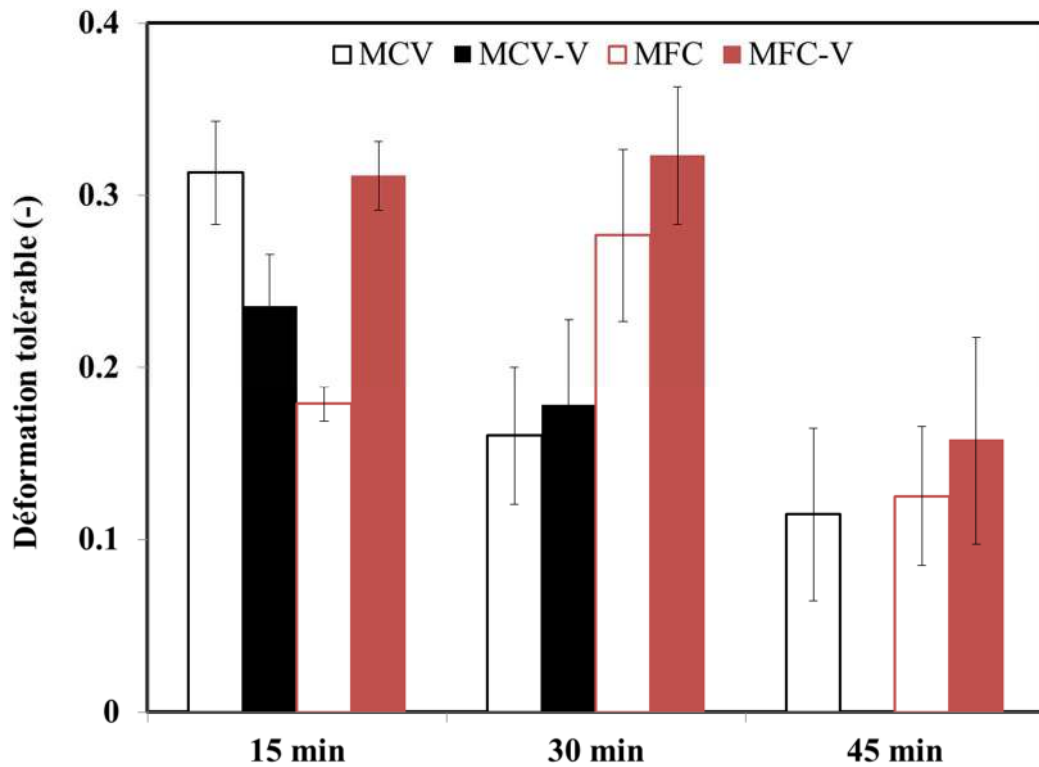
		MFA	MFA - V	MLF	MLF - V
15 min	Printed layers	14	18	11	13
	Pumping pressure (bar)	0.1	0.5	0.1	0.6
	Type of failure	Combined	Combined	Plastic collapse	Combined
	Predicted layer of failure	14	15	11	14
30 min	Printed layers	16	16	18	19
	Pumping pressure (bar)	0.2	1	0.1	0.6
	Type of failure	Buckling	Buckling	-	Buckling
	Predicted layer of failure	18	21	16	16
45 min	Printed layers	12	-	9	12
	Pumping pressure (bar)	0.4	-	0.4	1
	Type of failure	Buckling	-	Buckling	Buckling
	Predicted layer of failure	25	-	19	21



523

524

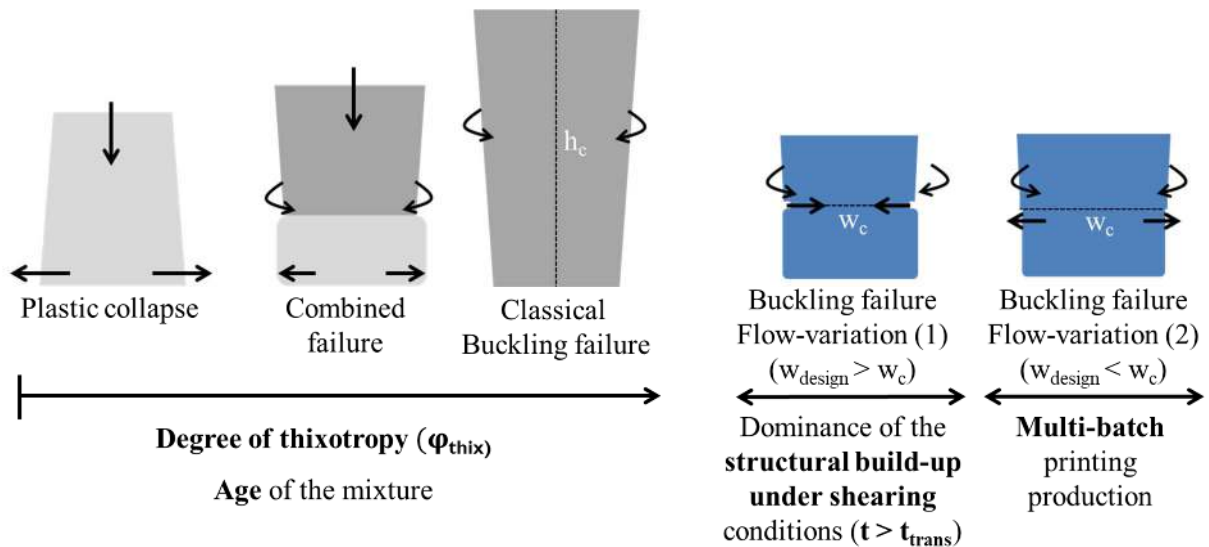
Fig. 19 : Printing quality control at 15, 30, and 45 min of age



525

526

Fig. 20 : Values of tolerable deformation at 15, 30, and 45 min of age



527

528

Fig. 21 : Types of failure in extrusion-based 3D printing

529

Conclusions

530

531

532

533

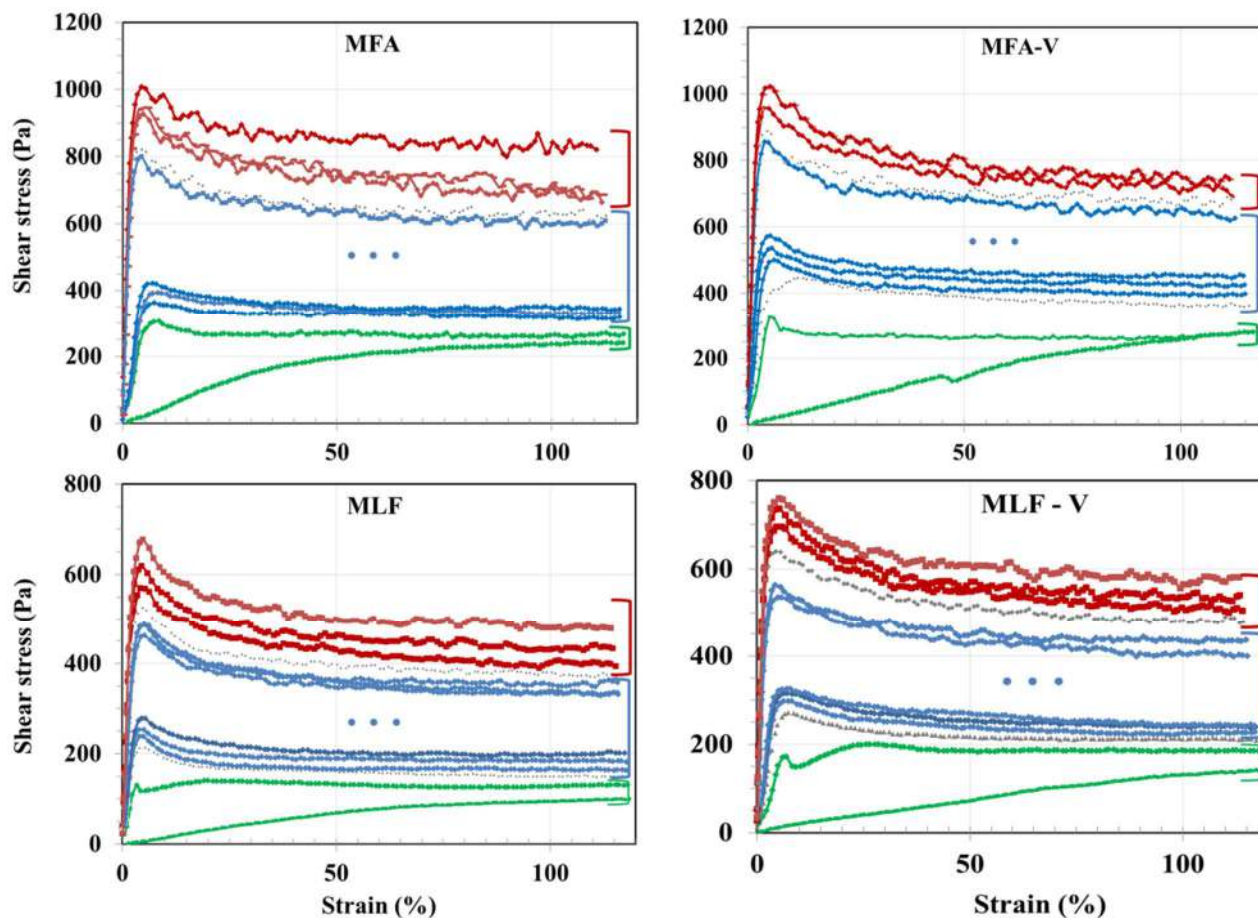
In this study, the time-dependent rheological properties of printable cement-based materials were investigated. Hysteresis loop tests were used to assess the time evolution of flow properties under shear conditions. The structural time-development properties were evaluated using yield stress growth and oscillatory tests. These properties contributed to controlling the printing

534 quality and highlighted the different instabilities that can occur during the printing process in
535 which continuous shear is applied during extrusion. Based on the reported results in this paper,
536 the following conclusions can be drawn:

- 537 (1) The rate of structuration A_{thix} did not provide sufficient information on the thixotropic
538 behavior of printable materials since it reflects only the material structuration at rest without
539 considering its time-dependent behavior during shearing conditions. This is more critical in
540 the case of single-batch production.
- 541 (2) The new thixotropy index φ_{thix} can be used to optimize the material design and printing
542 process by evaluating their printability window based on their kinetics of structuration under
543 different printing modes.
- 544 (3) Two stages of flow evolution were identified. The first stage can be monitored by the linear
545 increase of dynamic yield stress, while the second stage captures the exponential increase in
546 flow resistance due to flow loss.
- 547 (4) The competition between the break-down and the structural build-up affects the extrusion
548 quality over time, which can be reflected by the layer width reduction during printing.
- 549 (5) The determination of structural build-up evolution based on the growth of yield stress and
550 storage modulus development was found to be consistent at an early age. Beyond a certain
551 age, the storage modulus remains constant while the yield stress evolves continuously.
- 552 (6) The incorporation of a viscosity modifying agent enhanced the buildability of the
553 investigated mixtures. The effect of VMA was more pronounced on the rates of re-
554 flocculation R_{thix} and dynamic structuration B_{thix} than structuration A_{thix} and rigidification R .
- 555 (7) Buckling was the most frequent mode of failure due to flow variation effects. It is therefore
556 important to consider these variations when evaluating the stability of the printed structure.

557 **Acknowledgements**

558 The authors wish to thank the financial support of the National Science and Engineering
559 Research Council of Canada (NSERC) and the 8 industrial partners participating in the NSERC
560 Chair on development of Flowable Concrete with Adapted Rheology and their application in
561 concrete infrastructures, held by Professor Ammar Yahia at the University of Sherbrooke.

562 **Appendix A**

563

564 **Fig. A1** : Time evolution of the flow onset curves of the investigated mixtures – **Green**: Re-
 565 flocculation phase, **Blue**: Linear structuration, **Red**: Non-linear structuration, and **grey**:
 566 Transition phases

567 **References**

- 568 [1] T. Wangler *et al.*, « Digital Concrete: Opportunities and Challenges », *RILEM Technical*
 569 *Letters*, vol. 1, p. 67, oct. 2016, doi: 10.21809/rilemtechlett.2016.16.
- 570 [2] J. Xiao *et al.*, « Large-scale 3D printing concrete technology: Current status and future
 571 opportunities », *Cement and Concrete Composites*, vol. 122, p. 104115, sept. 2021, doi:
 572 10.1016/j.cemconcomp.2021.104115.
- 573 [3] V. Mechtcherine *et al.*, « Extrusion-based additive manufacturing with cement-based
 574 materials – Production steps, processes, and their underlying physics: A review », *Cement*
 575 *and Concrete Research*, vol. 132, p. 106037, juin 2020, doi:
 576 10.1016/j.cemconres.2020.106037.
- 577 [4] R. A. Buswell, W. R. Leal de Silva, S. Z. Jones, et J. Dirrenberger, « 3D printing using
 578 concrete extrusion: A roadmap for research », *Cement and Concrete Research*, vol. 112, p.
 579 37-49, oct. 2018, doi: 10.1016/j.cemconres.2018.05.006.

- 580 [5] F. Bos, R. Wolfs, Z. Ahmed, et T. Salet, « Additive manufacturing of concrete in
581 construction: potentials and challenges of 3D concrete printing », *Virtual and Physical*
582 *Prototyping*, vol. 11, n° 3, p. 209-225, juill. 2016, doi: 10.1080/17452759.2016.1209867.
- 583 [6] A. S. J. Suiker, R. J. M. Wolfs, S. M. Lucas, et T. A. M. Salet, « Elastic buckling and plastic
584 collapse during 3D concrete printing », *Cement and Concrete Research*, vol. 135, p. 106016,
585 sept. 2020, doi: 10.1016/j.cemconres.2020.106016.
- 586 [7] R. J. M. Wolfs et A. S. J. Suiker, « Structural failure during extrusion-based 3D printing
587 processes », *Int J Adv Manuf Technol*, vol. 104, n° 1, p. 565-584, sept. 2019, doi:
588 10.1007/s00170-019-03844-6.
- 589 [8] N. Roussel, « Rheological requirements for printable concretes », *Cement and Concrete*
590 *Research*, vol. 112, p. 76-85, oct. 2018, doi: 10.1016/j.cemconres.2018.04.005.
- 591 [9] A. Yahia, « Effect of solid concentration and shear rate on shear-thickening response of
592 high-performance cement suspensions », *Construction and Building Materials*, vol. 53, p.
593 517-521, févr. 2014, doi: 10.1016/j.conbuildmat.2013.10.078.
- 594 [10] Y. Jacquet, A. Perrot, et V. Picandet, « Assessment of asymmetrical rheological behavior of
595 cementitious material for 3D printing application », *Cement and Concrete Research*, vol.
596 140, p. 106305, févr. 2021, doi: 10.1016/j.cemconres.2020.106305.
- 597 [11] A. Perrot, D. Rangeard, et A. Pierre, « Structural built-up of cement-based materials used for
598 3D-printing extrusion techniques », *Materials and Structures*, vol. 49, n° 4, p. 1213-1220,
599 avr. 2016, doi: 10.1617/s11527-015-0571-0.
- 600 [12] P. Carneau, R. Mesnil, N. Ducoulombier, N. Roussel, et O. Baverel, « Characterisation of
601 the Layer Pressing Strategy for Concrete 3D Printing », in *Second RILEM International*
602 *Conference on Concrete and Digital Fabrication*, Cham, 2020, p. 185-195. doi:
603 10.1007/978-3-030-49916-7_19.
- 604 [13] M. Chen, L. Li, Y. Zheng, P. Zhao, L. Lu, et X. Cheng, « Rheological and mechanical
605 properties of admixtures modified 3D printing sulphoaluminate cementitious materials »,
606 *Construction and Building Materials*, vol. 189, p. 601-611, nov. 2018, doi:
607 10.1016/j.conbuildmat.2018.09.037.
- 608 [14] A. Prevedello Rubin, J. A. Hasse, et W. Longuini Repette, « The evaluation of rheological
609 parameters of 3D printable concretes and the effect of accelerating admixture »,
610 *Construction and Building Materials*, vol. 276, p. 122221, mars 2021, doi:
611 10.1016/j.conbuildmat.2020.122221.
- 612 [15] L. Reiter, T. Wangler, A. Anton, et R. J. Flatt, « Setting on demand for digital concrete –
613 Principles, measurements, chemistry, validation », *Cement and Concrete Research*, vol. 132,
614 p. 106047, juin 2020, doi: 10.1016/j.cemconres.2020.106047.
- 615 [16] M. Tramontin Souza *et al.*, « Role of chemical admixtures on 3D printed Portland cement:
616 Assessing rheology and buildability », *Construction and Building Materials*, vol. 314, p.
617 125666, janv. 2022, doi: 10.1016/j.conbuildmat.2021.125666.
- 618 [17] M. Papachristoforou, V. Mitsopoulos, et M. Stefanidou, « Evaluation of workability
619 parameters in 3D printing concrete », *Procedia Structural Integrity*, vol. 10, p. 155-162,
620 2018, doi: 10.1016/j.prostr.2018.09.023.
- 621 [18] L. Reiter, T. Wangler, N. Roussel, et R. J. Flatt, « The role of early age structural build-up in
622 digital fabrication with concrete », *Cement and Concrete Research*, vol. 112, p. 86-95, oct.
623 2018, doi: 10.1016/j.cemconres.2018.05.011.
- 624 [19] O. A. Mendoza Reales, P. Duda, E. C. C. M. Silva, M. D. M. Paiva, et R. D. T. Filho,
625 « Nanosilica particles as structural buildup agents for 3D printing with Portland cement
626 pastes », *Construction and Building Materials*, vol. 219, p. 91-100, sept. 2019, doi:
627 10.1016/j.conbuildmat.2019.05.174.

- 628 [20] F. P. Bos, P. J. Kruger, S. S. Lucas, et G. P. A. G. van Zijl, « Juxtaposing fresh material
629 characterisation methods for buildability assessment of 3D printable cementitious mortars »,
630 *Cement and Concrete Composites*, vol. 120, p. 104024, juill. 2021, doi:
631 10.1016/j.cemconcomp.2021.104024.
- 632 [21] J. Mewis et N. J. Wagner, « Thixotropy », *Advances in Colloid and Interface Science*, vol.
633 147-148, p. 214-227, mars 2009, doi: 10.1016/j.cis.2008.09.005.
- 634 [22] K. Dullaert et J. Mewis, « A structural kinetics model for thixotropy », *Journal of Non-
635 Newtonian Fluid Mechanics*, vol. 139, n° 1, p. 21-30, nov. 2006, doi:
636 10.1016/j.jnnfm.2006.06.002.
- 637 [23] H. Kanai et T. Amari, « Strain-thickening transition in ferric-oxide suspensions under
638 oscillatory shear », *Rheol Acta*, vol. 32, n° 6, p. 539-549, 1993, doi: 10.1007/BF00369070.
- 639 [24] D. Wang *et al.*, « Structural kinetics constitutive models for characterizing the time-
640 dependent rheologic behaviors of fresh cement paste », *Construction and Building
641 Materials*, vol. 276, p. 122175, mars 2021, doi: 10.1016/j.conbuildmat.2020.122175.
- 642 [25] Du J., Zhu W.W., Feng G.J., Liang W., Cshen X.G., et Xu C.F., « Rheological
643 characteristics of power-law cement grouts based on time-dependent behavior of viscosity »,
644 *Chemical Engineering Transactions*, vol. 51, p. 1111-1116, juill. 2016, doi:
645 10.3303/CET1651186.
- 646 [26] D. Wang *et al.*, « Study on dynamic and static structural build-up of fresh cement paste with
647 limestone powder based on structural kinetics model », *Construction and Building
648 Materials*, vol. 305, p. 124598, oct. 2021, doi: 10.1016/j.conbuildmat.2021.124598.
- 649 [27] A. M. Mostafa et A. Yahia, « New approach to assess build-up of cement-based
650 suspensions », *Cement and Concrete Research*, vol. 85, p. 174-182, juill. 2016, doi:
651 10.1016/j.cemconres.2016.03.005.
- 652 [28] S. Ma, Y. Qian, et S. Kawashima, « Experimental and modeling study on the non-linear
653 structural build-up of fresh cement pastes incorporating viscosity modifying admixtures »,
654 *Cement and Concrete Research*, vol. 108, p. 1-9, juin 2018, doi:
655 10.1016/j.cemconres.2018.02.022.
- 656 [29] I. Harbouz, E. Roziere, A. Yahia, et A. Loukili, « Physico-Chemical Characterization at
657 Early-Age of 3D Printed Mortar », in *Second RILEM International Conference on Concrete
658 and Digital Fabrication*, Cham, 2020, p. 272-279. doi: 10.1007/978-3-030-49916-7_28.
- 659 [30] D. Jiao, R. De Schryver, C. Shi, et G. De Schutter, « Thixotropic structural build-up of
660 cement-based materials: A state-of-the-art review », *Cement and Concrete Composites*, vol.
661 122, p. 104152, sept. 2021, doi: 10.1016/j.cemconcomp.2021.104152.
- 662 [31] N. Roussel, « A thixotropy model for fresh fluid concretes: Theory, validation and
663 applications », *Cement and Concrete Research*, vol. 36, n° 10, p. 1797-1806, oct. 2006, doi:
664 10.1016/j.cemconres.2006.05.025.
- 665 [32] P. C. F. Møller, J. Mewis, et D. Bonn, « Yield stress and thixotropy: on the difficulty of
666 measuring yield stresses in practice », *Soft Matter*, vol. 2, n° 4, p. 274, 2006, doi:
667 10.1039/b517840a.
- 668 [33] I. Ivanova et V. Mechtcherine, « Evaluation of Structural Build-Up Rate of Cementitious
669 Materials by Means of Constant Shear Rate Test: Parameter Study », in *Rheology and
670 Processing of Construction Materials*, Cham, 2020, p. 209-218. doi: 10.1007/978-3-030-
671 22566-7_25.
- 672 [34] Quemada Daniel, *Modélisation rhéologique structurelle: dispersions concentrées et fluides
673 complexes / Daniel Quemada,...* Paris: Éd. Tec & Doc Lavoisier, 2006.
- 674 [35] J. Kruger, S. Zeranka, et G. van Zijl, « An ab initio approach for thixotropy characterisation
675 of (nanoparticle-infused) 3D printable concrete », *Construction and Building Materials*, vol.
676 224, p. 372-386, nov. 2019, doi: 10.1016/j.conbuildmat.2019.07.078.

- 677 [36] N. Roussel, « Thixotropie des bétons modernes : Modélisation et application », in *XXVIèmes*
678 *Rencontres Universitaires de Génie Civil AUGC 2008*, France, juin 2008, p. 9p. Consulté le:
679 15 août 2022. [En ligne]. Disponible sur: <https://hal.archives-ouvertes.fr/hal-00400539>
- 680 [37] I. Harbouz, E. Roziere, A. Yahia, et A. Loukili, « Printability assessment of cement-based
681 materials based on rheology, hydration kinetics, and viscoelastic properties », *Construction*
682 *and Building Materials*, vol. 325, p. 126810, mars 2022, doi:
683 10.1016/j.conbuildmat.2022.126810.
- 684 [38] N. Roussel, G. Ovarlez, S. Garrault, et C. Brumaud, « The origins of thixotropy of fresh
685 cement pastes », *Cement and Concrete Research*, vol. 42, n° 1, p. 148-157, janv. 2012, doi:
686 10.1016/j.cemconres.2011.09.004.
- 687 [39] G. De Schutter et D. Feys, « Pumping of Fresh Concrete: Insights and Challenges », *RILEM*
688 *Technical Letters*, vol. 1, p. 76, nov. 2016, doi: 10.21809/rilemtechlett.2016.15.
- 689 [40] R. Wolfs, T. Salet, et N. Roussel, « Filament geometry control in extrusion-based additive
690 manufacturing of concrete: The good, the bad and the ugly », *Cement and Concrete*
691 *Research*, vol. 150, p. 106615, déc. 2021, doi: 10.1016/j.cemconres.2021.106615.
- 692 [41] I. Harbouz, « Impression 3D des matériaux cimentaires », *Academic Journal of Civil*
693 *Engineering*, vol. 39, n° 1, p. 169-176, mai 2021.
- 694 [42] A. W. Saak, H. M. Jennings, et S. P. Shah, « The influence of wall slip on yield stress and
695 viscoelastic measurements of cement paste », *Cement and Concrete Research*, vol. 31, n° 2,
696 p. 205-212, févr. 2001, doi: 10.1016/S0008-8846(00)00440-3.
- 697 [43] A. M. Mostafa, P. Diederich, et A. Yahia, « Effectiveness of rotational shear in dispersing
698 concentrated cement suspensions », *Journal of Sustainable Cement-Based Materials*, vol. 4,
699 n° 3-4, p. 205-214, oct. 2015, doi: 10.1080/21650373.2015.1010659.
- 700 [44] A. Yahia et K. H. Khayat, « Analytical models for estimating yield stress of high-
701 performance pseudoplastic grout », *Cement and Concrete Research*, vol. 31, n° 5, p.
702 731-738, mai 2001, doi: 10.1016/S0008-8846(01)00476-8.
- 703 [45] A. M. Mostafa et A. Yahia, « Performance Evaluation of Different Rheometric Shearing
704 Techniques to Disperse Concentrated Cement Suspension », *Applied Rheology*, vol. 25, n° 3,
705 p. 23–31, 2015, doi: 10.3933/applrheol-25-34337.
- 706 [46] H. Bessaies-Bey, K. H. Khayat, M. Palacios, W. Schmidt, et N. Roussel, « Viscosity
707 modifying agents: Key components of advanced cement-based materials with adapted
708 rheology », *Cement and Concrete Research*, vol. 152, p. 106646, févr. 2022, doi:
709 10.1016/j.cemconres.2021.106646.
- 710 [47] F. J. Rubio-Hernández, J. M. Morales-Alcalde, et A. I. Gómez-Merino, « Limestone
711 filler/cement ratio effect on the flow behaviour of a SCC cement paste », *Advances in*
712 *Cement Research*, vol. 25, n° 5, p. 262-272, oct. 2013, doi: 10.1680/adcr.12.00027.
- 713 [48] P. Billberg, « Form Pressure Generated by Self-Compacting Concrete — Influence of
714 Thixotropy and Structural Behaviour at Rest », p. 105.
- 715 [49] A. Baldan, « Review Progress in Ostwald ripening theories and their applications to nickel-
716 base superalloys Part I: Ostwald ripening theories », *Journal of Materials Science*, vol. 37,
717 n° 11, p. 2171-2202, juin 2002, doi: 10.1023/A:1015388912729.
- 718 [50] M. Palacios et R. J. Flatt, « 20 - Working mechanism of viscosity-modifying admixtures »,
719 in *Science and Technology of Concrete Admixtures*, P.-C. Aïtcin et R. J. Flatt, Éd.
720 Woodhead Publishing, 2016, p. 415-432. doi: 10.1016/B978-0-08-100693-1.00020-5.
- 721 [51] K. H. Khayat, « Viscosity-enhancing admixtures for cement-based materials — An
722 overview », *Cement and Concrete Composites*, vol. 20, n° 2, p. 171-188, janv. 1998, doi:
723 10.1016/S0958-9465(98)80006-1.

- 724 [52]Z. H. Ou, B. G. Ma, et S. W. Jian, « Influence of cellulose ethers molecular parameters on
725 hydration kinetics of Portland cement at early ages », *Construction and Building Materials*,
726 vol. 33, p. 78-83, août 2012, doi: 10.1016/j.conbuildmat.2012.01.007.
- 727 [53]R. Bouras, A. Kaci, et M. Chaouche, « Influence of viscosity modifying admixtures on the
728 rheological behavior of cement and mortar pastes », *Korea-Aust. Rheol. J.*, vol. 24, n° 1, p.
729 35-44, mars 2012, doi: 10.1007/s13367-012-0004-3.
- 730 [54]S. Chaves Figueiredo, O. Çopuroğlu, et E. Schlangen, « Effect of viscosity modifier
731 admixture on Portland cement paste hydration and microstructure », *Construction and*
732 *Building Materials*, vol. 212, p. 818-840, juill. 2019, doi:
733 10.1016/j.conbuildmat.2019.04.020.
- 734 [55]H. Green et R. N. Weltmann, « Equations of Thixotropic Breakdown for Rotational
735 Viscometer », *Ind. Eng. Chem. Anal. Ed.*, vol. 18, n° 3, p. 167-172, mars 1946, doi:
736 10.1021/i560151a004.
- 737 [56]D. K. Panesar et R. Zhang, « Performance comparison of cement replacing materials in
738 concrete: Limestone fillers and supplementary cementing materials – A review »,
739 *Construction and Building Materials*, vol. 251, p. 118866, août 2020, doi:
740 10.1016/j.conbuildmat.2020.118866.
- 741 [57]E. Roziere, R. Cortas, et A. Loukili, « Tensile behaviour of early age concrete: New
742 methods of investigation », *Cement and Concrete Composites*, vol. 55, p. 153-161, janv.
743 2015, doi: 10.1016/j.cemconcomp.2014.07.024.
- 744 [58]Q. Yuan, D. Zhou, K. H. Khayat, D. Feys, et C. Shi, « On the measurement of evolution of
745 structural build-up of cement paste with time by static yield stress test vs. small amplitude
746 oscillatory shear test », *Cement and Concrete Research*, vol. 99, p. 183-189, sept. 2017, doi:
747 10.1016/j.cemconres.2017.05.014.
748